DOE/PC/79903--T17

DOE/PC/79903--T17

DE93 001870

OPTICAL PROPERTIES OF FLYASH

Contract No. DE-AC22-87PC 79903

Quarterly Report for Period 1 April – 30 June 1989

Prepared for Pittsburgh Energy Technology Center

Principal Investigator Professor S. A. Self

DISCLAIMER

July 1989

HIGH TEMPERATURE GASDYNAMICS LABORATORY
Mechanical Engineering Department
Stanford University

OPTICAL PROPERTIES OF FLYASH
Contract No. DE-AC22-87PC 79903
Quarterly Report for Period 1 April – 30 June 1989
Prepared for Pittsburgh Energy Technology Center
Principal Investigator Professor S. A. Self

EXECUTIVE SUMMARY

The general aims of this research are to provide a fundamental scientific basis for the physical understanding and reliable calculation of radiative heat transfer in coal combustion systems, particularly as it is influenced by the presence of inorganic constituents deriving from the mineral matter in coal.

The work is organized under four tasks. Tasks I and II were initiated in October 1987; Tasks III and IV were funded from October 1988.

Task 1. Characterization of Flyash: Under this heading the chemical composition and size distribution of representative flyashes are being measured by appropriate microanalytical techniques to provide information required in Task 2.

Task 2. Measurements of the Optical Constants of Slags: Under this heading measurements of the infrared optical constants (i.e., the complex refractive index $m = n - ik$) of synthetic slags are being made as a function of wavelength and temperature for controlled compositions. Particular attention will be given to the contribution of the Fe_2O_3 content and its valence state. The data is being reduced to yield formulae giving the complex refractive index over relevant ranges of wavelength and temperature, as a function of the relevant metal oxide constituents.

Task 3. Sample Calculations of the Radiant Properties of Flyash Dispersions: This component comprises various calculations to guide and evaluate the experimental work under the other three tasks.

Task 4. Measurement of the Radiant Properties of Flyash Dispersions: This bench-scale experiment is planned to compare the measured radiant properties of a dispersion of well-characterized ash with computations based on data developed under the first two tasks.

In this seventh quarter good progress has been made in all four areas, as reported in the Quarterly Report, and summarized below.

Task 1

The ashes being characterized are samples from power plants or pilot-scale combustors derived from combustion of the same seven coals selected for study under the parallel PETC program on "Transformation of Inorganic Coal Constituents in Combustion Systems."

The principal features requiring characterization are particle size and composition distributions, including correlations between size and composition. Size distributions are being measured in house by Coulter counter. Size and composition distributions are being determined by automated SEM/microprobe analysis at UNDERC. Other in-house characterization work under way includes size classification by wet sieving combined with classification by density using flotation/sedimentation techniques, low temperature ashing for the char content and magnetic separation for the magnetite content resulting from combustion of pyrite.

During the past quarter, size distributions for four of the ashes over the range 0.5 – 60 μm were completed using the Coulter multisizer with a technique employing two orifices to cover the whole range. A suitable technique for matching distributions using two orifice sizes was devised. The measured distribution was found to be very well represented by truncated log-normal distributions. For the other ashes, having a significant fraction of larger particles, a similar technique using three separate orifices will be used.

Micrographs of the ash samples prepared by UNDERC for automated SEM/EDX size-composition analysis revealed many agglomerates, casting some doubt on the validity of the data. A freeze-drying technique for sample preparation has been developed at Stanford which gives very well dispersed samples. The automated SEM/EDX analysis has been repeated using such samples and the results are currently being analyzed using statistical computer codes developed at Stanford.

In addition, this quarter, experiments to perfect the techniques for density classification and magnetic separation of flyash have been performed.

Task 2

Methods for determining the infrared optical properties of solid synthetic and natural slags at low temperatures have been established in prior work at Stanford. In the present work the main effort has been devoted to the development of suitable apparatus and techniques for performing similar measurements on slags at temperatures to 2000K, when the slag is liquid. Basic experimental strategies have been decided and apparatus has been designed to accomplish this task. Preliminary tests at high temperatures during past quarters have resulted in the first reliable measurements of the infrared absorption of liquid slag.

Two complementary techniques involving infrared optical measurements on liquid samples of synthetic slag maintained in an electric furnace are being developed. The first, for the wavelength range 1 – 5 μm where the absorption index is low ($k \leq 10^{-2}$) employs a submerged platinum mirror to measure the absorption of thin films of slag by a double-pass technique. The second, applicable over the whole wavelength range (1–12 μm), measures the surface reflectance of the liquid slag relative to that of a cold gold mirror in an external reference path.

The first technique has been successfully used to obtain the first reliable measurements of the infrared absorption of liquid slag (at 2000 K).

In the past quarter, efforts have been concentrated on developing and testing the second technique (for surface reflectivity measurements). It was determined that the quality of the data obtained is limited by the differing absorptions due to CO_2 and H_2O in the hot measurement path and the cold reference path. To eliminate this problem, the whole apparatus has been enclosed in a chamber, purged with dry nitrogen.

With this modification, good measurements of the reflectivity of synthetic slag containing 5% Fe at 1600°C were made over the whole wavelength range 1–12 μm. The data in the range 8–12 μm were reduced, using the Kramers–Kronig technique to give both the real and imaginary parts of the complex refractive index. These measurements constitute the first reliable measurements of the infrared optical constants of molten slag.

Task 3

Programs have been written for Mie scattering calculations which are then convolved with input on the size and optical constants distributions for a particulate dispersion to yield the spectral scattering and absorption coefficients of the aerosol. Additionally, a program has been written to solve the radiation transfer problem for a homogeneous slab, utilizing the exact solution method of Case's normal modes. Input for the spectral scattering and absorption coefficients from the first program allows the spectral scattering, absorption and emission properties of the slab to be computed. These can then be integrated over wavelength to yield the total radiative heat transfer characteristics of the slab.

These programs have been used to determine the importance of certain features of typical ashes for radiation transfer. These include the sensitivity of the optical/radiative properties of a flyash dispersion to (i) composition-size correlation, especially with regard to the distribution of iron oxides with particle size, and (ii) the presence of bubbles in the glassy ash particles.

This computational capability is also being used to evaluate the experimental conditions in the design of the apparatus for Task 4.

Task 4

In the past quarter, careful consideration has been given to the feasibility of various basic approaches for implementing the goals of this task. After evaluating various experimental techniques, a basic approach has tentatively been identified. This will be firmed up by design calculations and preliminary tests during the next quarter.

1.0 INTRODUCTION

This is the sixth quarterly report under DOE contract No. DE-AC22-87PC 79903 entitled "Optical Properties of Flyash." Tasks 1 and 2 of this program were funded from 15 September 1987. Tasks 3 and 4 were funded from 15 September 1988.

The general aims of this research are to provide a fundamental scientific basis for the physical understanding and reliable calculation of radiative heat transfer in coal combustion systems, particularly as it is influenced by the presence of inorganic constituents deriving from the mineral matter in coal. Some preliminary work in this area has been carried out at Stanford in the past several years with NSF support. The present program will greatly enlarge the scope of this work.

The complete, integrated program of theoretical and experimental work comprises four separate tasks.

Task 1. Characterization of Flyash

Task 2. Measurements of the Optical Constants of Slags

Task 3. Sample Calculations of the Radiant Properties of Flyash Dispersions.

Task 4. Measurements of the Radiative Properties of Flyash Dispersions.

In Task 1, the chemical composition and size distribution of representative flyashes are being measured by appropriate microanalytical techniques to provide information required in Tasks 2 and 3.

In Task 2, measurements of the infrared optical constants (i.e., the complex refractive index $m = n - ik$) of synthetic slags are being made as a function of wavelength and temperature for controlled compositions. Particular attention is being given to the contribution of Fe_2O_3 content and its valence state. The data will be reduced to yield formulae giving the complex refractive index over relevant ranges of wavelength and temperature, as a function of the relevant metal oxide constituents.

In Task 3, sample calculations are being made for typical ash loadings, size distributions and compositions for simple geometries, with two main purposes: first, to provide insight and physical understanding of the role of flyash in radiative heat transfer in combustion systems; second, to indicate the sensitivity of the results to the characteristics of the input data. Such calculations will also be used to determine appropriate conditions and to predict the expected measured radiative properties for the experiment of Task 4.

The experiment of Task 4 is designed to critically test our ability to predict the measured spectral emittance and scattering coefficient of flyash dispersions under well-controlled laboratory conditions utilizing the optical property data developed in Task 2. Particular attention will be paid to assessing the contribution of the char component in typical ashes. Any discrepancies between calculated and measured quantities revealed by these tests will be resolved by appropriate further studies.

A more detailed description of the scope of these tasks is given below. First, however, an outline is given of the rationale for the overall approach adopted in this program.

1.1 Rationale of Overall Approach

To account for the effects of flyash in radiative heat transfer calculations requires a knowledge of the contributions of the ash to the spectral absorption (a_λ) and scattering (σ_λ) coefficients of the particulate dispersion, together with the phase function Φ_λ describing the anisotropy of the scattering. These quantities depend on the particulate loading as well as the distributions of the size and optical properties of the particles.

For a spherical particle of homogeneous, optically isotropic material, characterized by a complex refractive index $m \equiv (n - ik)$ Mie theory allows one to compute the spectral absorption ($Q_{\lambda,a}$) and scattering ($Q_{\lambda,s}$) efficiencies of the particle, as well as the phase function ϕ_λ. For randomly polarized radiation, these quantities are a function of the particle size parameter $x \equiv (\pi d/\lambda)$, and the complex refractive index $m(C, \lambda, T)$, a function of composition, wavelength and temperature.

For a monodispersion of identical spherical particles, of specified loading (i.e. number density), the particulate's contribution to the optical properties (a_λ, σ_λ and Φ_λ) of the medium are simply related to the spectral properties ($Q_{\lambda,a}$, $Q_{\lambda,s}$, ϕ_λ) of a single particle. It is also straightforward to compute the spectral optical properties of the medium for a polydispersion of spheres of identical composition, by convolving the results of Mie calculations for spheres of varying diameter (i.e. x) for fixed wavelength (and hence fixed m), with the particle size distribution (assumed given). In the case of a particulate material, like flyash, for which it is reasonable to assume that individual particles are of homogeneous composition but the composition varies from particle to particle, it is still possible to compute the spectral characteristics of the particulate dispersion by dividing the particles into an appropriate number of classes of varying composition (and hence m), each having a specified size distribution, and summing over particle classes.

In radiative heat transfer calculations, the contribution of the gas to the spectral absorption coefficient is added to that of the particles to obtain the combined optical properties of the medium on a spectral basis. These optical properties are then used as input for a radiation transfer code to calculate radiative fluxes, on a spectral basis, for a particular combustor geometry and boundary conditions. Finally, to obtain total heat transfer quantities such as the overall radiant heat flux, integrations over wavelength must be made.

The procedure, outlined above, represents the only logical approach to the computation of radiative heat transfer in flyash laden combustion gases. To implement this procedure requires, as input, a detailed characterization of the ash with respect to its size and (complex) refractive index distributions on a spectral basis.

Now, while techniques are available for determining the size distribution of powder samples, such as flyash, there are no practical means available for reliably determining the complex refractive index distribution of a complex material such as flyash either on a single particle basis, as a powder or as a dispersed aerosol. However, it is possible, using modern microanalytical techniques, specifically computer-automated SEM/EDX analysis, to determine the size and chemical composition of a heterogeneous powder on a particle by particle basis for a statistically large number of particles.

If the compositions of individual particles can be related to the complex refractive index of their material, then the characterization of a particular ash in terms of its size and composition distributions can lead to the necessary input for carrying out the calculations, outlined above, to compute radiation transfer in combustion systems containing that ash.

Thus the key requirement, necessary for the implementation of this approach, is data on the optical constants (i.e. the components n, k of the complex refractive index) as a function of composition, wavelength and temperature covering the range of compositions found in representative ashes. Since, as noted above, and emphasized in texts on the optical properties of particulate matter, it is impractical to extract reliable data on the optical constants of material in particulate form, the only viable approach is to make measurements on homogeneous bulk samples for which well-established techniques are available.

The foregoing arguments provide the rationale for the present program. Characterization of representative flyashes concerning their size and composition distributions constitutes Task 1, while measurements of the optical constants on bulk samples of synthetic slags as a function of relevant ranges of composition, wavelength and temperature constitute Task 2. Task 3 is designed to provide computational capabilities to support the other tasks, while Task 4 is planned to provide an experimental test that the measured optical properties of a dispersion of flyash can indeed be computed reliably from a knowledge of the size and composition distributions of the ash.

1.2 Description of Tasks

TASK 1 - Characterization of Flyash

Extensive prior analyses of flyash from a wide range of coals plus analyses of the mineral matter in raw coals, together with knowledge of the transformation processes occurring during combustion, lead to the following overall picture of the nature of flyash.

The particle size distribution is very broad with a volume (or mass) mean diameter on the order of 10 μm. Typically it is well represented by a log normal distribution with the 1% and 99% sizes in a cumulative plot by volume occurring at ~1 μm and 70 μm respectively. Evidence of a distinct submicron fume due to homogeneous condensation of volatile mineral matter is sometimes found, but this fraction can be expected to contribute negligibly to radiation transfer.

With regard to chemical composition, several distinct classes of particle can be identified and plausibly related to their origin and formation mechanisms.

By far the preponderant class, usually representing on the order of 90% or more of the ash on a mass basis, consists of vitreous (amorphous) material composed primarily of SiO_2, Al_2O_3, CaO_2 and MgO, usually in that order, but containing varying smaller percentages of other metal oxides, notably Fe_2O_3. It can appropriately be identified as particles of impure (calcium) aluminosilicate glass derived from the microscopic clay-like mineral inclusions in the coal matrix. As char burnout proceeds these inclusions melt and form liquid globules on the surface of the char (which they do not wet) and are then released into the gas.

These glassy particles tend to be quite spherical with smooth surfaces and of reasonably homogeneous composition as is to be expected from their formation as liquid droplets. As they cool after release from the char surface, they remain in the vitreous state because the cooling rate is much faster than the crystallization rate for the formation of specific phases. The fact that the bulk of most ashes consists of reasonably spherical, homogeneous and vitreous (and therefore optically isotropic) particles is a very fortunate fact, since they satisfy the assumptions of the Mie theory remarkably well.

Micrographs of optically polished sections of ash cast in epoxy resin, shows that these glassy particles sometimes contain a number of small bubbles of gas evolved from the char and trapped in the particles as they form on the char surface. More rarely, large, thin-walled cenospheres are observed which presumably are "glass-blown" when a liquid drop covers a pore in the char from which a relatively large volume of gas is evolved under pressure. Although such cenospheres are very prominent objects in micrographs, their number is usually too small to significantly affect radiation transfer.

Auger spectroscopic studies of ash often show a thin surface layer composed of volatile metals and high in sulfur (as sulfates) and water. The presence of a thin layer of adsorbed water containing sulfate ions controls the electrical resistance of the surface which is very important in the performance of electrostatic precipitators. However, this surface layer, of different composition from the underlying particle, is too thin (≤100Å) relative to wavelengths of interest to affect the optical properties of the particle.

Apart from this major class of glassy particles, several distinct minor classes of particle types can be identified, each comprising, at most, a few percent by mass of the flyash. One such class consists of incompletely burned char particles which are clearly identified in optical and SEM micrographs by the fact that they are black, of irregular shape and porous. The mass fraction of char depends on the particular coal and the combustor configuration and operating conditions. In modern combustors the mass fraction of unburned char is normally a few percent at most.

Another minor class consists of particles of adventitious incombustible mineral matter (e.g. quartz) which is contained in the pulverized coal feed. Such particles are usually large and of irregular shape, often showing rounded edges indicating partial melting.

A third minor class consists of magnetite (Fe_3O_4) which derives from the combustion of pyrite (FeS_2) particles contained in the coal grind. These magnetite particles are black, generally spherical, magnetic and much denser than the glassy particles. The proportion of magnetite particles depends on the coal type, being largest in high sulfur coals, because the sulfur is mostly associated with pyrite. Recent work has shown that much of the pyrite in the coal grind can be removed by washing/sedimentation with a reduction in SO_x emissions as high as 50% in some high sulfur coals.

The ashes selected for characterization are samples from power plants or pilot-scale combustors derived from the same seven coals selected for study under the parallel PETC program on "Transformation of Inorganic Coal Constituents in Combustion Systems" which comprise four bituminous, one sub-bituminous and two lignite coals.

A variety of techniques are being used in the characterization of these ashes. The principal method for determining size distributions employs a Coulter Multisizer which is capable of giving accurate, reliable results of high resolution over a wide dynamic range ≤1 μm to ≥ 100 μm.

Automated, computer-controlled, combined SEM/EDX microanalysis will be the principal technique used to determine the distributions of composition and size for a large number (~1000) of particles for each ash. The size distributions will be compared with those obtained by the Coulter counter.

Other techniques to be used include classification by density using liquids of varying density in a centrifuge, together with classification by size using a wet-sieving method. These techniques can yield density and size separated fractions for further examination by microanalytical techniques such as energy-dispersive X-ray spectroscopy. In addition, the magnetite particles may be separated by magnetic separation. The char content will be determined by low temperature ashing.

TASK 2 - Measurements of Optical Constants of Synthetic Slags

This task is planned to provide the basic optical properties data in a comprehensive and conveniently usable form. The optical constants (i.e., the components of the complex refractive index $m = n - ik$) of samples of synthetic slags of controlled compositions will be measured using established techniques involving transmission and surface reflectance methods. The wavelength range will extend from the visible to 12 μm, and the temperature range will extend to 2000K.

In earlier work at Stanford, supported by NSF, extensive measurements of this type were made on polished wafers of synthetic slags at temperatures up to 1200 K. A major component of this task will be to extend such measurements to higher temperatures (~2000 K) where the slag is liquid. This requires the development of modified techniques which present a number of more or less severe technical challenges.

Initially, the optical constants of the basic calcium-aluminosilicate host glass will be determined for the composition range defined by Task 1. Subsequently, by adding infrared-active mineral oxide constituents in controlled amounts, one at a time, the modifications to $m(\lambda, T)$ produced by such constituents will be quantitatively determined. The particular constituents (and their range of mass fractions) to be examined will be determined by those disclosed by Task 1, taking account of knowledge of the optical activity at relevant wavelengths of such additions from the literature of glass technology. Specific constituents to be examined will include Fe_2O_3, taking especial account of its valence state (Fe^{2+}/Fe^{3+} ratio), and of TiO_2. The contribution of the OH radical to the optical properties will be evaluated and quantified if significant.

The experimental data on $m(\lambda, T)$ as a function of composition, over the range relevant to coal ashes, will be reduced to generate simple correlation formulae. The latter will constitute the data base necessary to calculate the radiative properties of bulk slags and ash dispersions required for understanding and computing radiative transfer in coal combustion systems.

TASK 3 - Sample Calculations of the Radiant Properties of Flyash Dispersions

This task is intended to provide computational capabilities to support the other tasks. It includes the following components.

(i) A Mie scattering code to calculate the absorption and scattering efficiencies and phase function of a single sphere of specified size parameter and complex refractive index. A modified Mie code will also allow such computations for hollow spheres.

(ii) A code to convolve the results from (i) over a specified size distribution and loading to compute the absorption and scattering coefficients and phase function of a homogeneous polydispersion.

(iii) A code to sum the results of (ii) for a number of classes of particles of varying refractive indices and size distributions, i.e. for a heterogeneous polydispersion.

(iv) A radiation transfer code to calculate the absorption, scattering and emission characteristics of a homogenous, isothermal slab of dispersed ash on a spectral basis.

(v) A code to integrate the spectral results from (iv) over wavelength to yield the total radiative properties of the slab.

Calculations using these codes will be used to provide sensitivity analyses to guide the characterization work of Task 1, and to design and evaluate the results of Task 4.

TASK 4 - Measurement of the Radiative Properties of Flyash Dispersions

The purpose of this laboratory scale experiment is to test our ability to predict the measured radiative properties of a dispersion of well-characterized flyash. As such it will provide a critical test of the effectiveness of the overall approach adopted in this program.

2.0 PROGRESS IN THE PAST QUARTER

2.1 Task 1: Characterization of Flyash

Size Distribution by Coulter Multisizer:

In the last QPR, we described in detail a procedure for combining Coulter Multisizer data obtained using orifice tubes of two different sizes. In future, this procedure will be used for all flyash sizing. For those ashes received from Foster-Wheeler, it was found that a 30 μm and a 100 μm orifice tube were sufficient to span the full range of particle size. This expanded range extends from 1.2 μm to about 60 μm. The best-fit log-normal function, *truncated* outside this extended measurement range, has been fitted to the data. This size distribution function can be expressed mathematically as:

$$f(d) = \left[\frac{1}{\sqrt{2\pi}\cdot d\cdot \ln \sigma_g} \exp\left\{-\left(\frac{\ln d/d_n}{2 \ln \sigma_g}\right)^2\right\}\right] \Big/ \text{cum}; \quad a \le d \le b$$

where

$$\text{cum} = \frac{1}{\sqrt{2\pi}\cdot d\cdot \ln \sigma_g} \int_a^b \exp\left[-\left(\frac{\ln x/d_n}{2 \ln \sigma_g}\right)^2\right] dx$$

and

$$f(d) = 0 \qquad d < a \quad \text{and} \quad d > b$$

where

d	=	particle diameter
a	=	lower limit of size measurement (= 1.2 μm)
b	=	largest size for which particles were detected
d_n	=	median diameter
σ_g	=	geometric standard deviation
x	=	dummy variable of integration

The reason for using a truncated log-normal function is that we cannot measure particles outside the size range 'a' to 'b'. Hence, the distribution should be normalized by the integral term 'cum'. If it were possible to measure all possible particle sizes, the term 'cum' would have a value of unity.

By replacing the diameter term, d, in the equation by surface area, s, or volume, v, one can obtain the area and volume distributions respectively. One can then define a median diameter, d_S, based on surface area distribution or a median diameter d_V, based on volume distribution given by

$$s_g = \pi\, d_S^2, \text{ and } v_g = \pi\, d_V^3 / 6$$

where

$$s_g = \text{median surface area and } v_g = \text{median volume}$$

The three median diameters are related as follows:

$$\ln d_S = \ln d_n + 2.0(\ln \sigma_g)^2$$

$$\ln d_V = \ln d_n + 3.0(\ln \sigma_g)^2$$

The geometric standard deviation is the same for all three distributions. This is a special property of the log-normal distribution.

The best-fit truncated log-normal function was computed by minimizing the r.m.s. error between the function and the data using Nelder and Mead's multidimensional downhill simplex method for function minimization [Reference 1]. It is an iterative procedure which converges in approximately two minutes on the 80286 PC. The guessed values which initiate the computation are obtained from the data. The 50% size is used as the estimated median value. For the geometric standard deviation, the ratio of the sizes corresponding to 84% undersize to 16% undersize is used as the guessed value. At the end of computation, the computer program outputs the median diameter and σ_g corresponding to the best-fit function.

As Figure 1 shows, the truncated log-normal distribution function fits the data quite well. Another way of presenting the data is shown in Figure 2. Here, using the best-fit log-normal function, the distribution of particles down to a size of 0.1 μm has been calculated. This *assumes* that the particles with diameter smaller than 1.2 μm follow the same truncated log-normal distribution. On the cumulative plot in Figure 2, the contributions to the volume, by these 'particles', have been added to the data points. The points now lie on a straight line on the log-probability plot. In this manner, we have removed the artifact discussed in

Size Distribution of Flyash Plotted on Log-Probability Axes

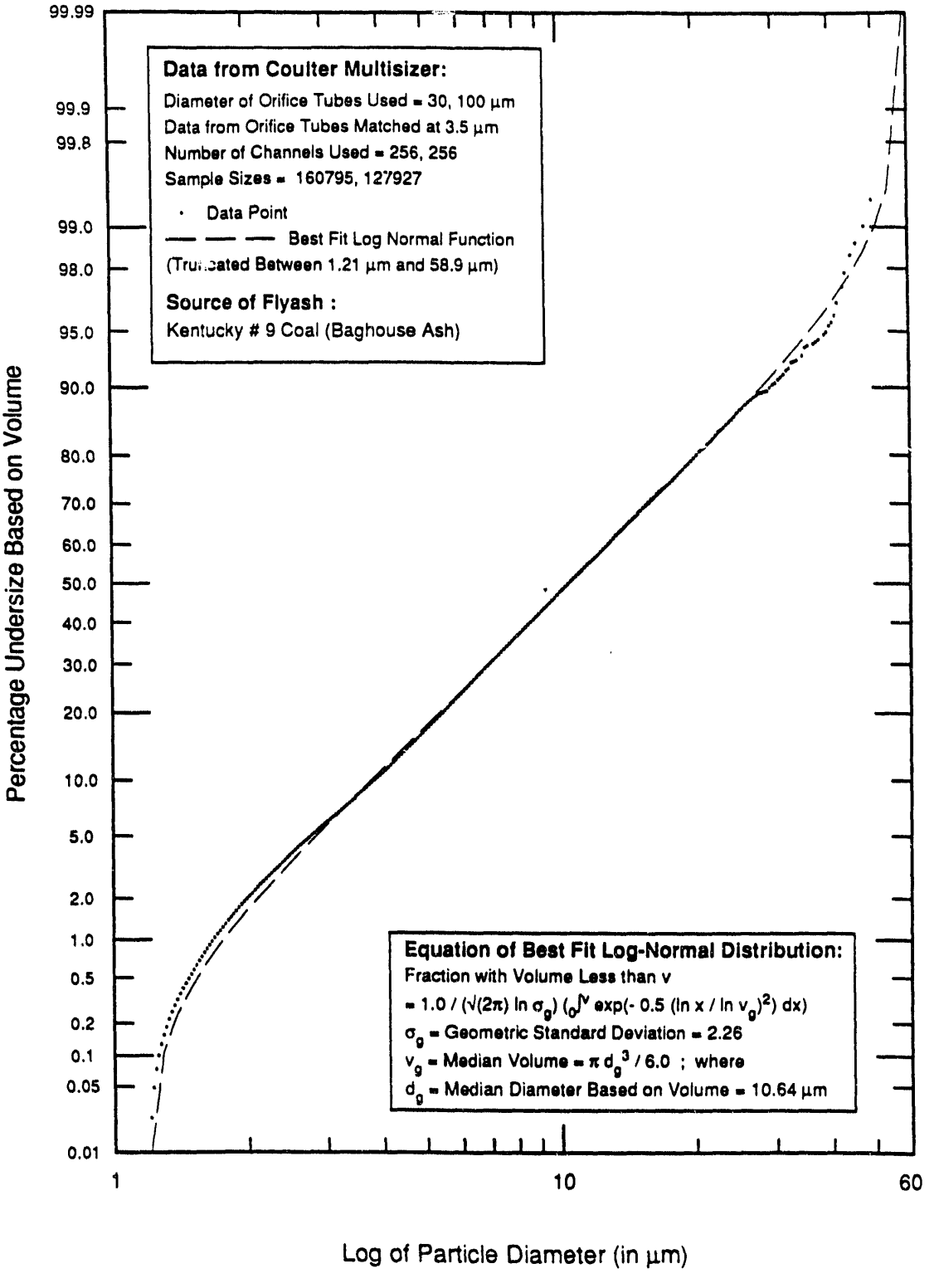

Figure 1

Size Distribution of Flyash Plotted on Log-Probability Axes

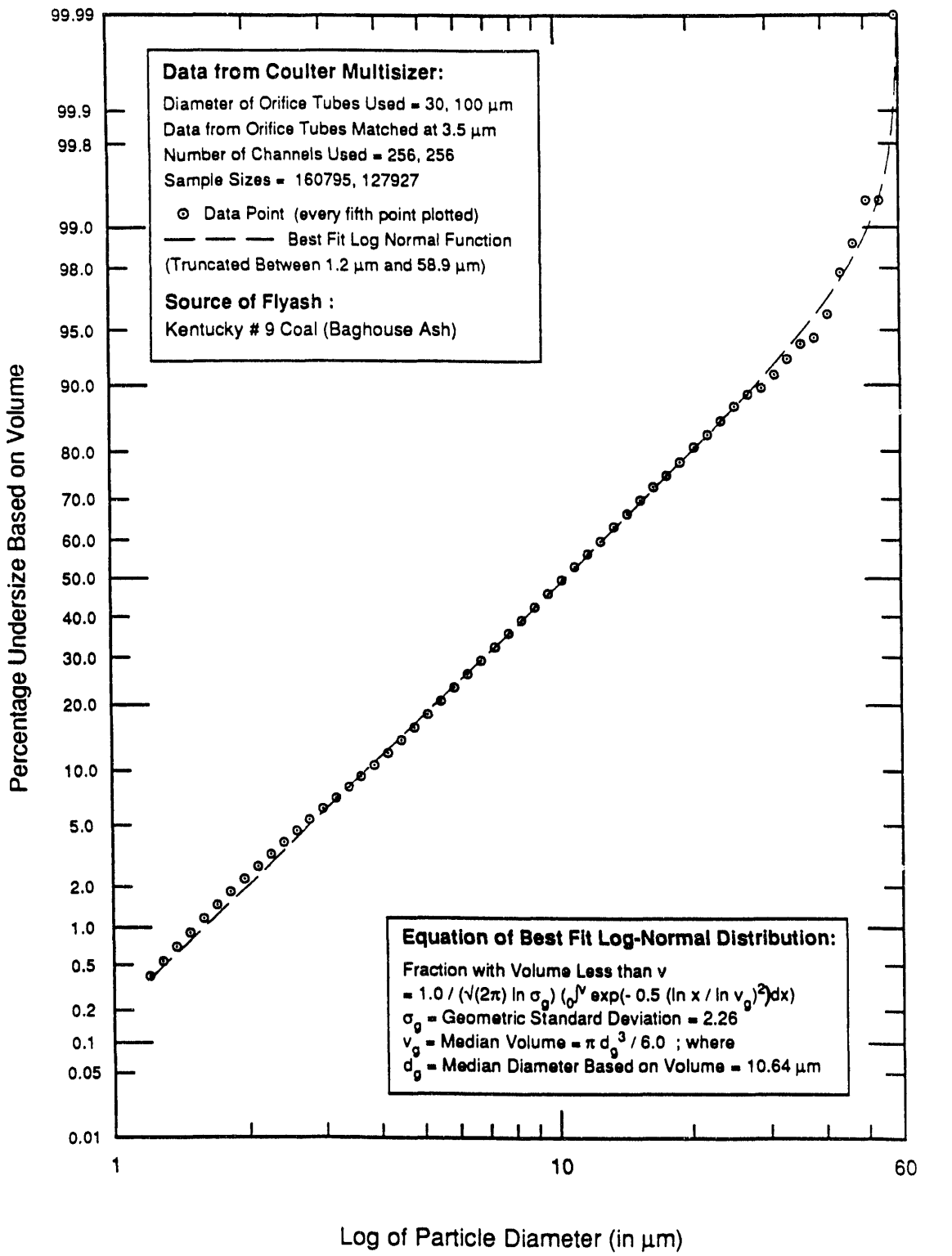

07-27-89

Figure 2

previous quarterly reports whereby there was an apparent departure of the size distribution from a log normal function close to the lower limit of measurement. This, of course, resulted from the inability to measure particle sizes below 1.2 μm but could have been misconstrued by the reader to imply that the smaller particles did not follow a log-normal distribution.

Considering that it is unlikely that the ash follows a distinctly different size distribution in the sub-micron region, it is reasonable to expect a single log-normal function to characterize the ash size distribution over the entire range of interest. Hence, we will assume that the truncated log-normal can predict the number of particles below 1.2 μm when there is a need to define the ash size distribution over a wider range of sizes. We are exploring the possibility of either (1) digitizing SEM micrographs and sizing the particles using an edge detection algorithm or (2) preparing slides of the micrographs and enlarging them by projecting them on a screen. Either of these techniques will help in checking the accuracy of the above stated assumption.

No effort has been made to extend the log-normal function beyond the upper size limit and force the data points to lie on a straight line. This is because the frequency of the distribution is very low at these sizes (i.e., there are very few large particles) and there is a large statistical scatter about the log-normal line (see Figure 3 for a frequency plot on a log size scale). In fact, this scatter can be reduced by using fewer than 256 channels because there would be more particles sampled per channel. However, 256 channels have been used because they yield more data points which in turn gives a more accurate best-fit log-normal function. Moreover, there are large numbers of particles sampled in the smaller size intervals.

It should be realized that the 50% size read off from the cumulative size distribution plot represents the median size only when the function is truncated symmetrically about the median size. In the case of asymmetrical truncation, as in the case here, the median corresponding to the best fit truncated log-normal function is slightly different from the 50% size shown on the graph (see Figure 4).

Figures 5-11 show data for the four ashes supplied by Foster Wheeler. The remaining two ashes are currently being sized using data from three different orifice tubes. These ashes are from full scale power plants (San Miguel and Eagle Butte) and have larger median diameters and geometric standard deviations than the other four which are from a pilot scale combustor.

In Figure 5, size distributions based on diameter, surface area and volume are shown on the same plot. A property of the log normal distribution is that these three related distributions lie on parallel straight lines on a log-probability graph. Figure 6 shows data on

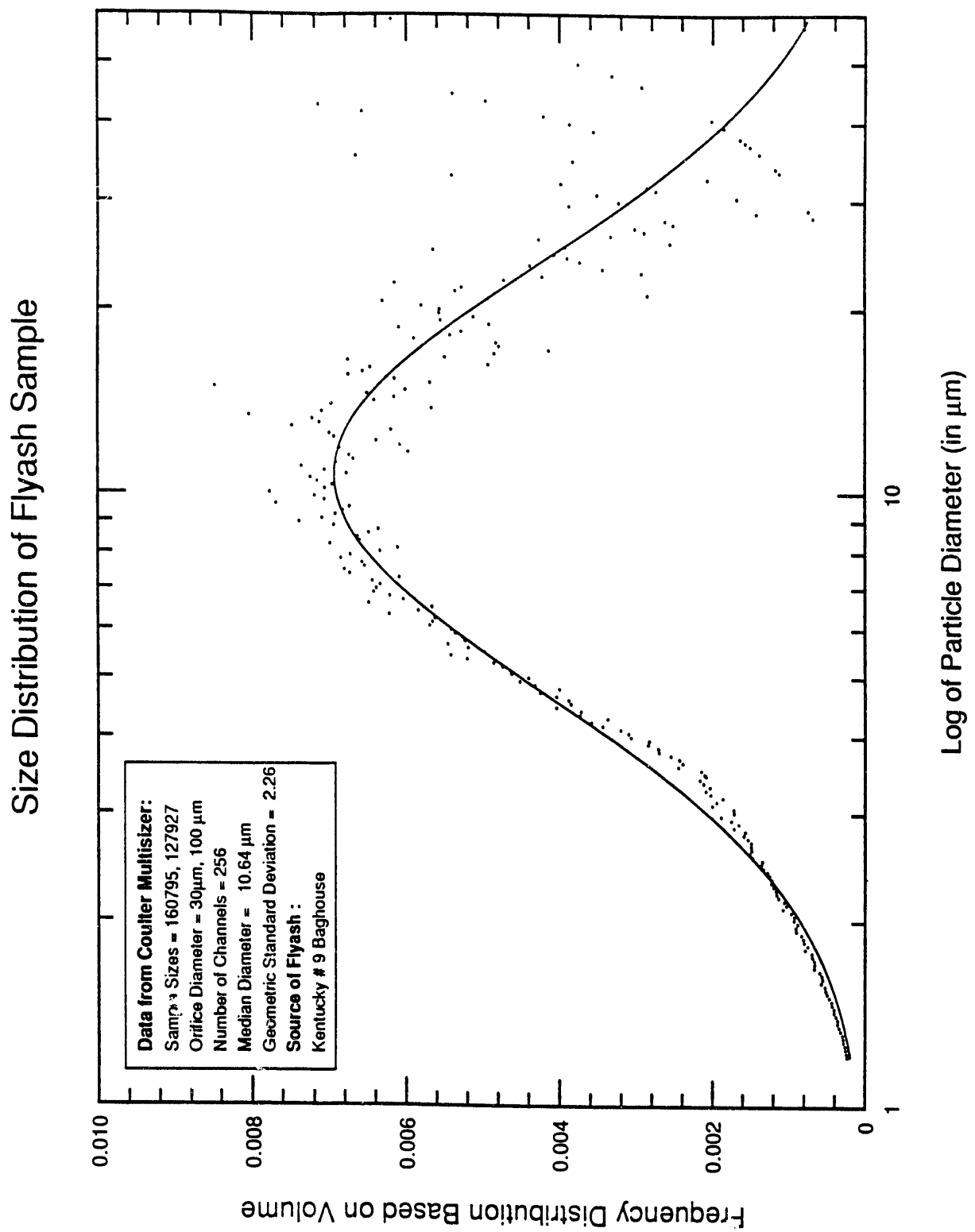
Size Distribution of Flyash Sample
Data from Coulter Multisizer:
Sample Sizes = 160795, 127927
Orifice Diameter = 30µm, 100 µm
Number of Channels = 256
Median Diameter = 10.64 µm
Geometric Standard Deviation = 2.26
Source of Flyash :
Kentucky # 9 Baghouse
Frequency Distribution Based on Volume
0.010
0.008
0.006
0.004
0.002
0
1
10
Log of Particle Diameter (in µm)

Figure 3

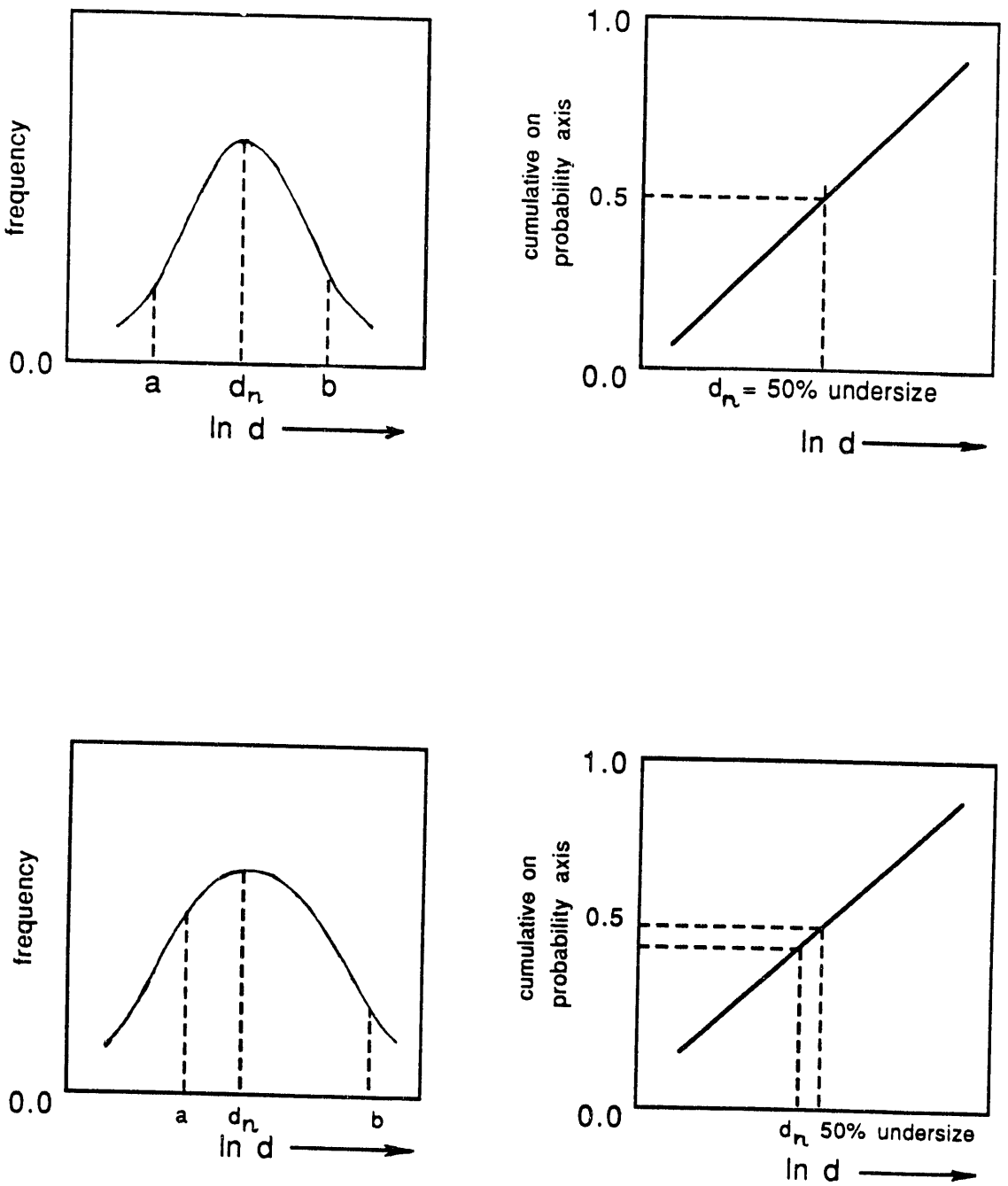

Figure 4: Log-normal Distribution

Size Distribution of Flyash Plotted on Log-Probability Axes

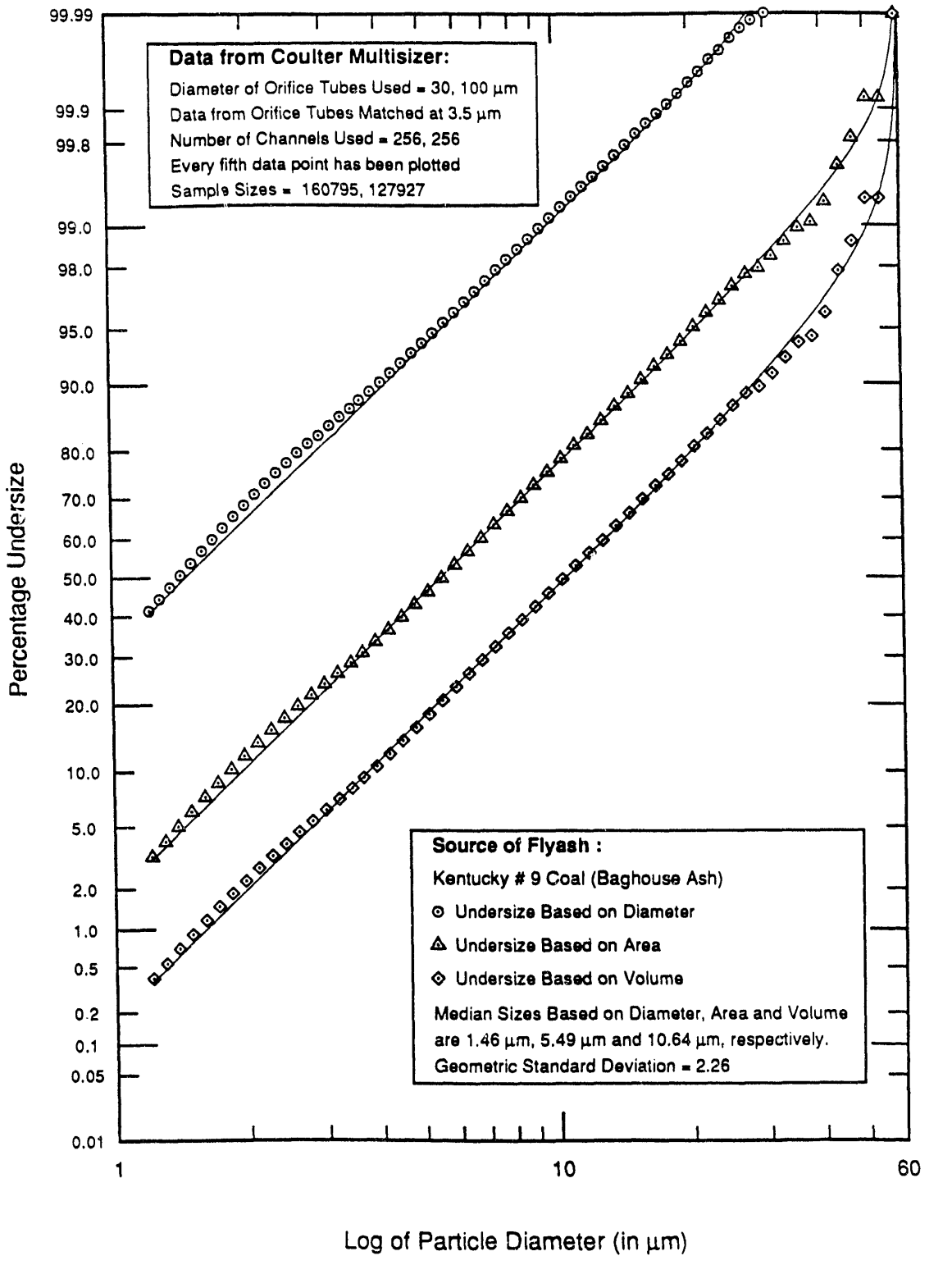

Figure 5

Size Distribution of Flyash Plotted on Log-Probability Axes

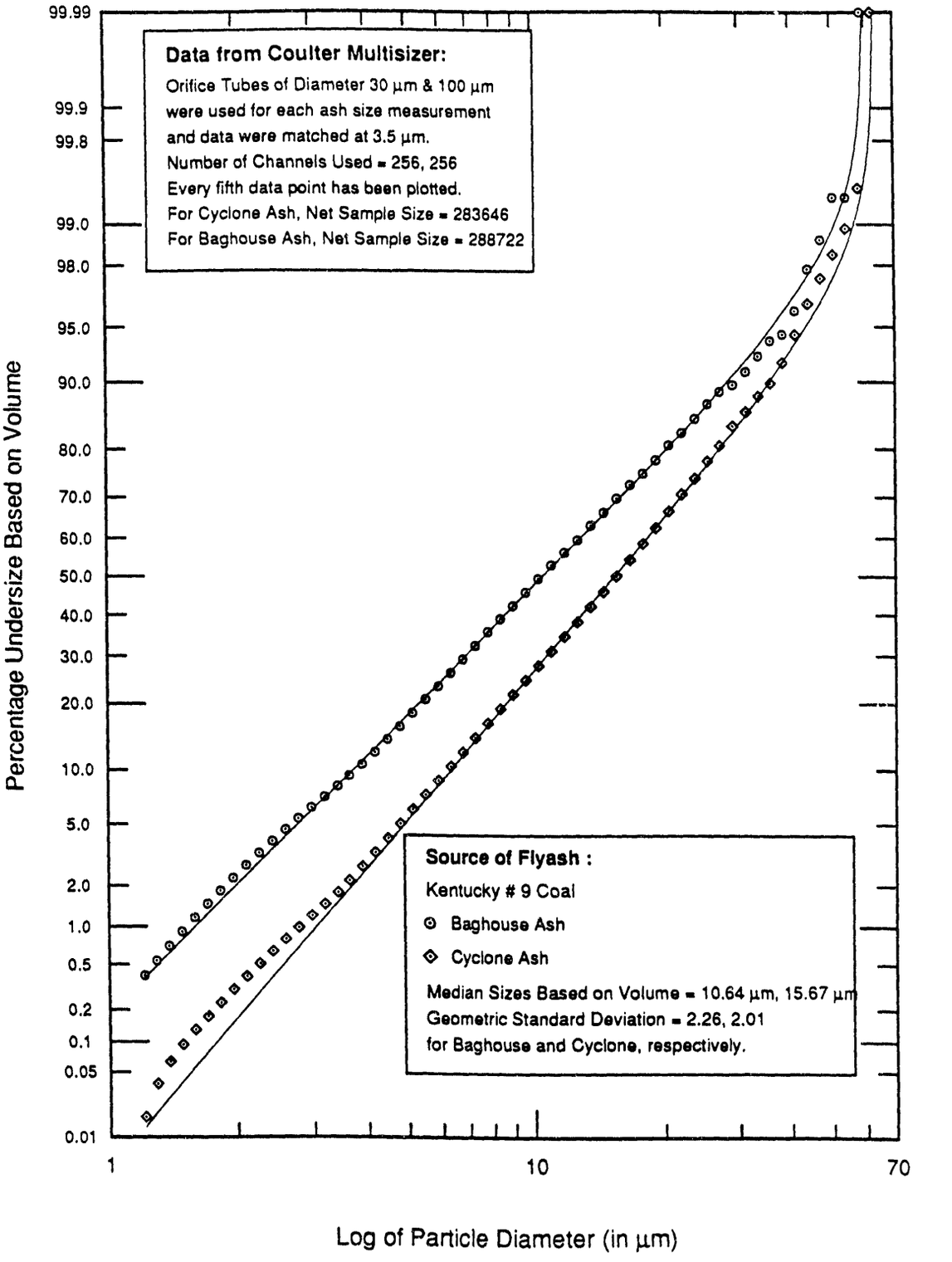

07-27-89

Figure 6

Size Distribution of Flyash Plotted on Log-Probability Axes

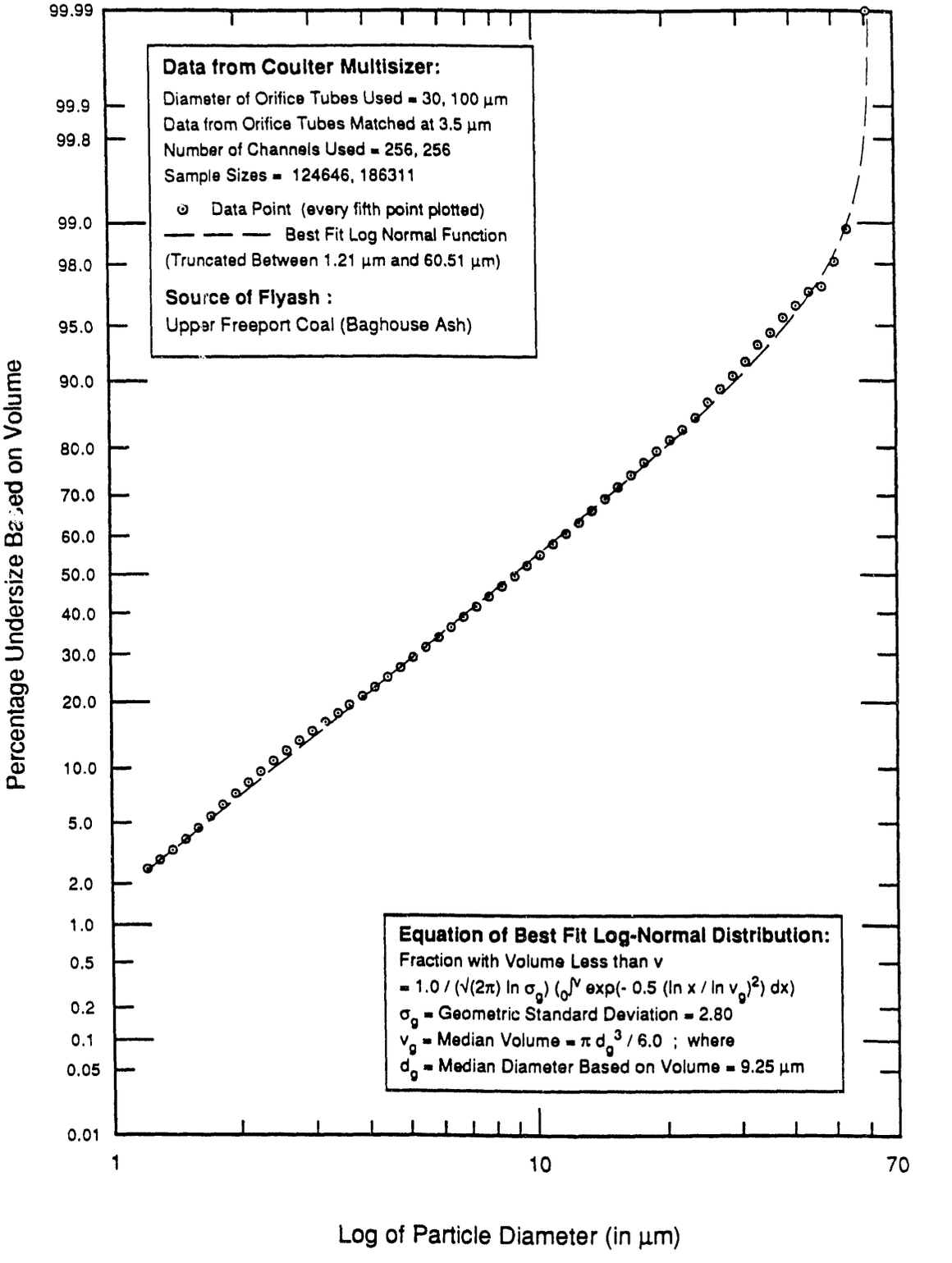

Figure 7

Size Distribution of Flyash Plotted on Log-Probability Axes

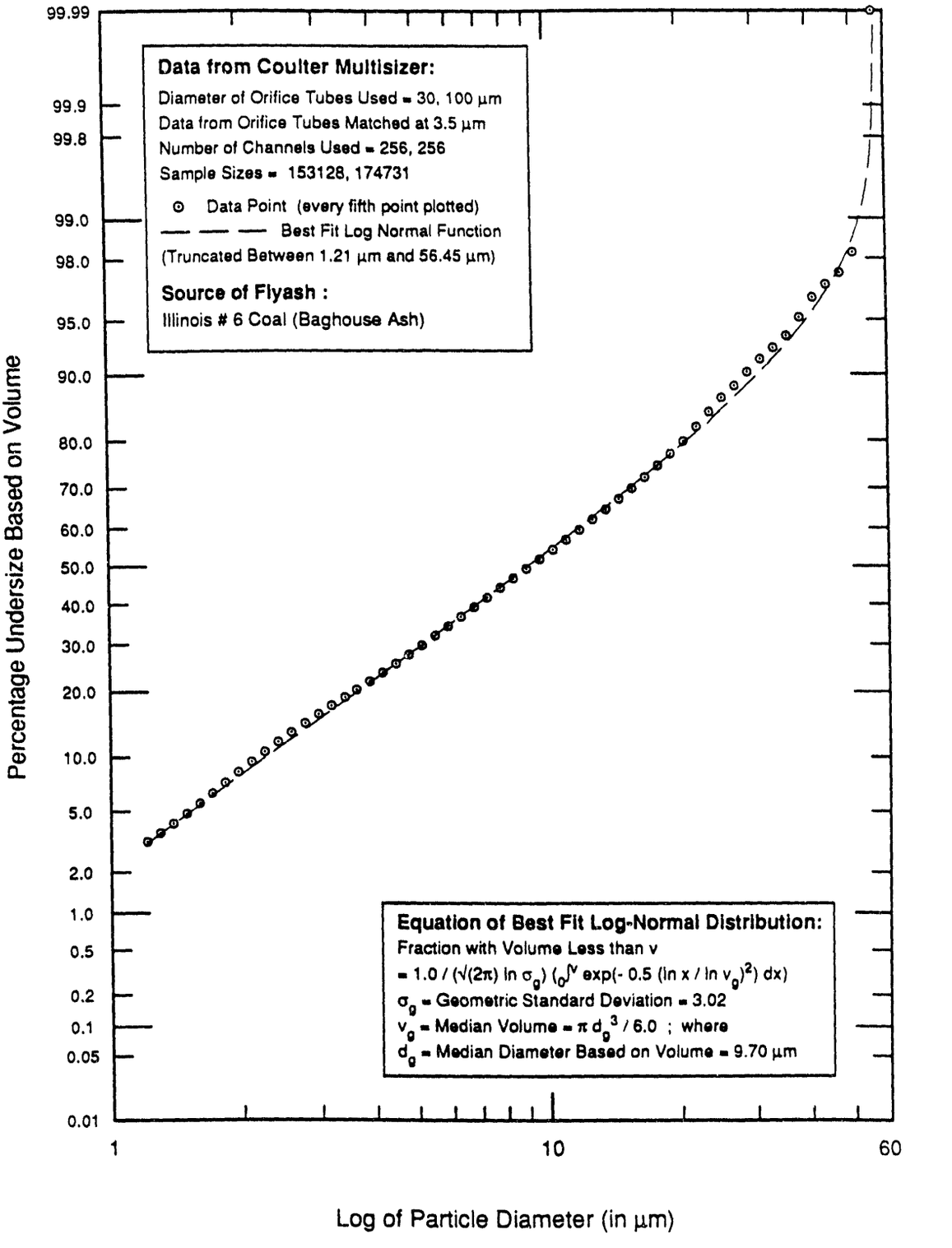

Figure 8

Size Distribution of Flyash Plotted on Log-Probability Axes

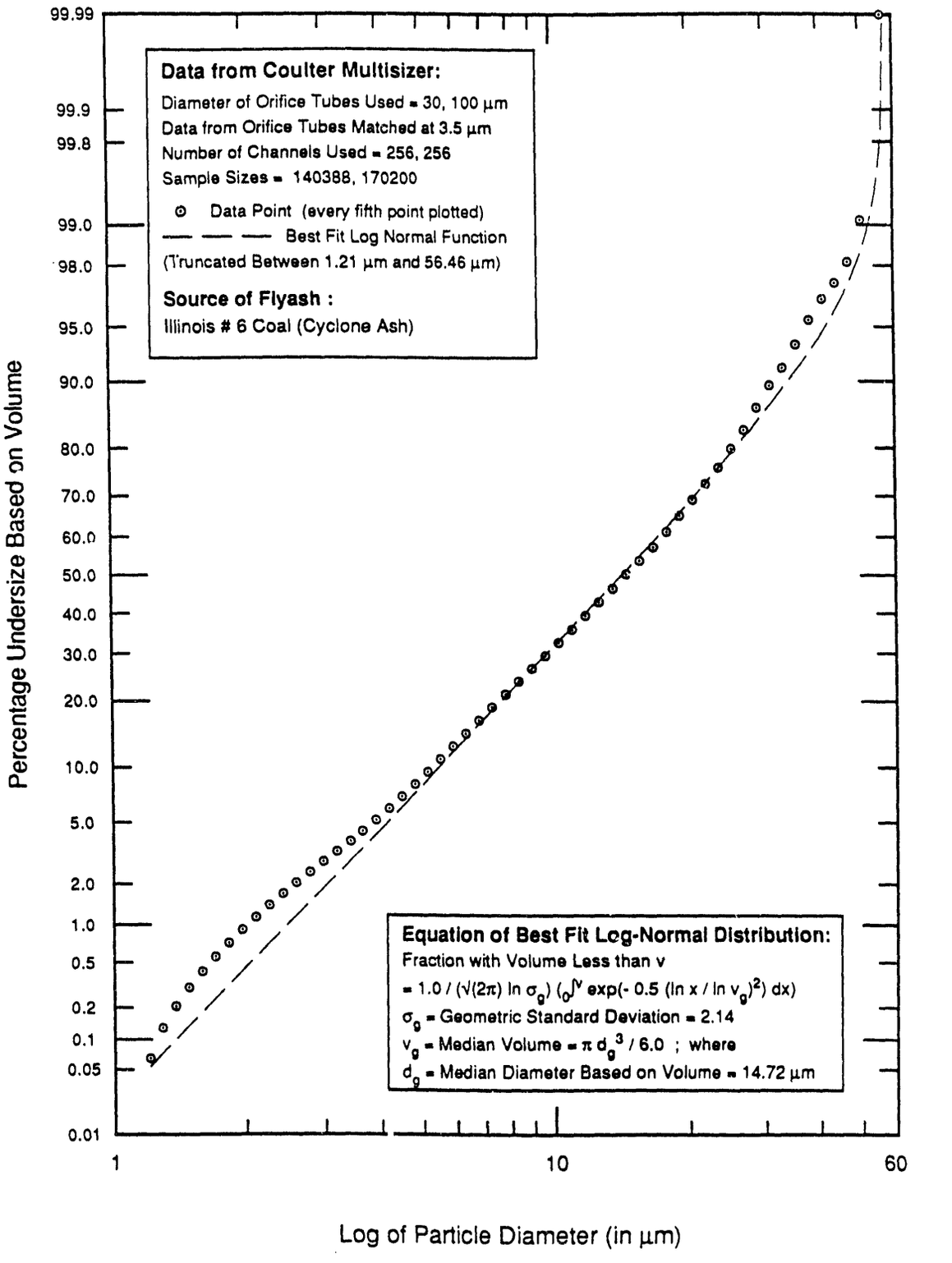

07-27-89

Figure 9

Size Distribution of Flyash Plotted on Log-Probability Axes

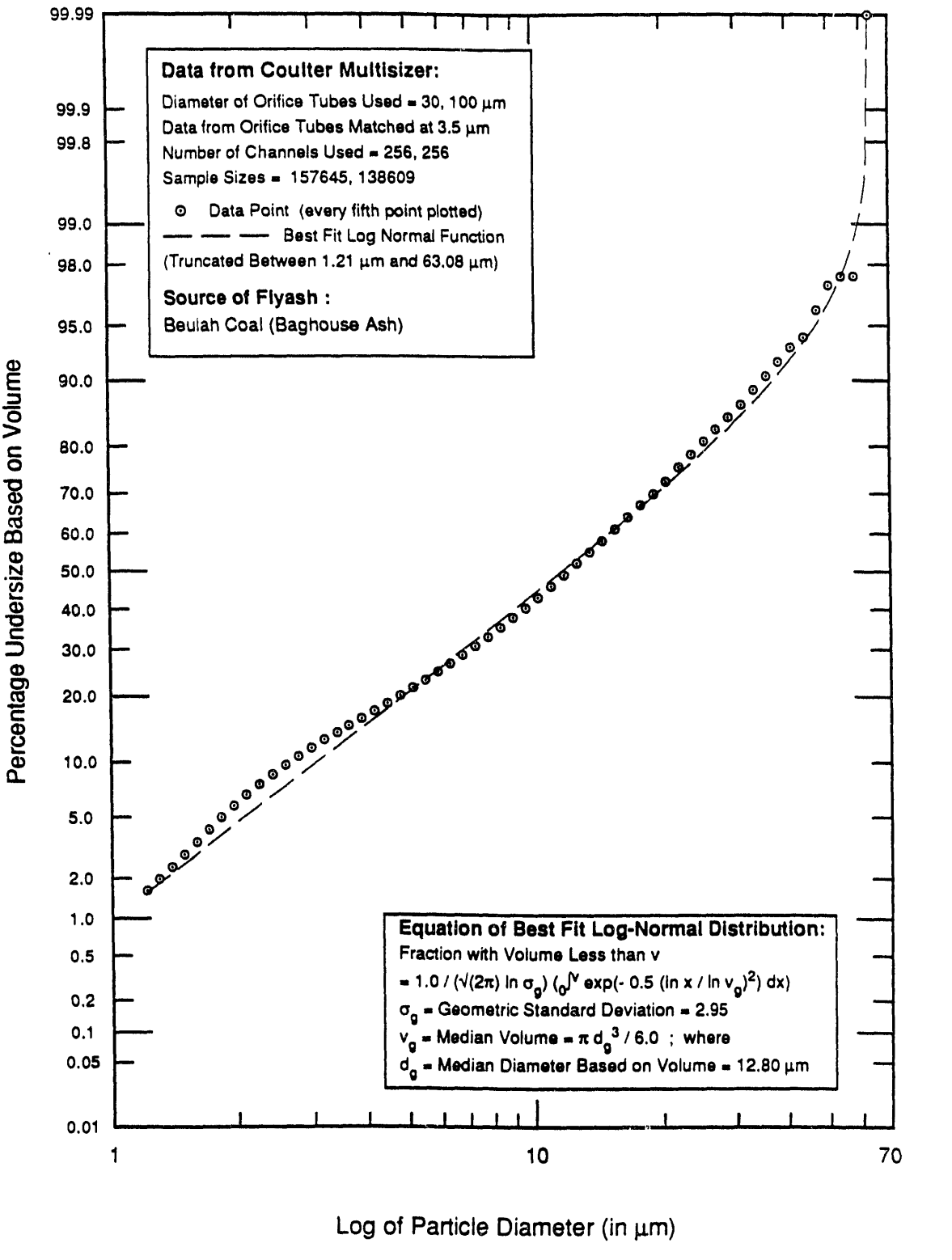

07-27-89

Figure 10

Size Distribution of Flyash Plotted on Log-Probability Axes

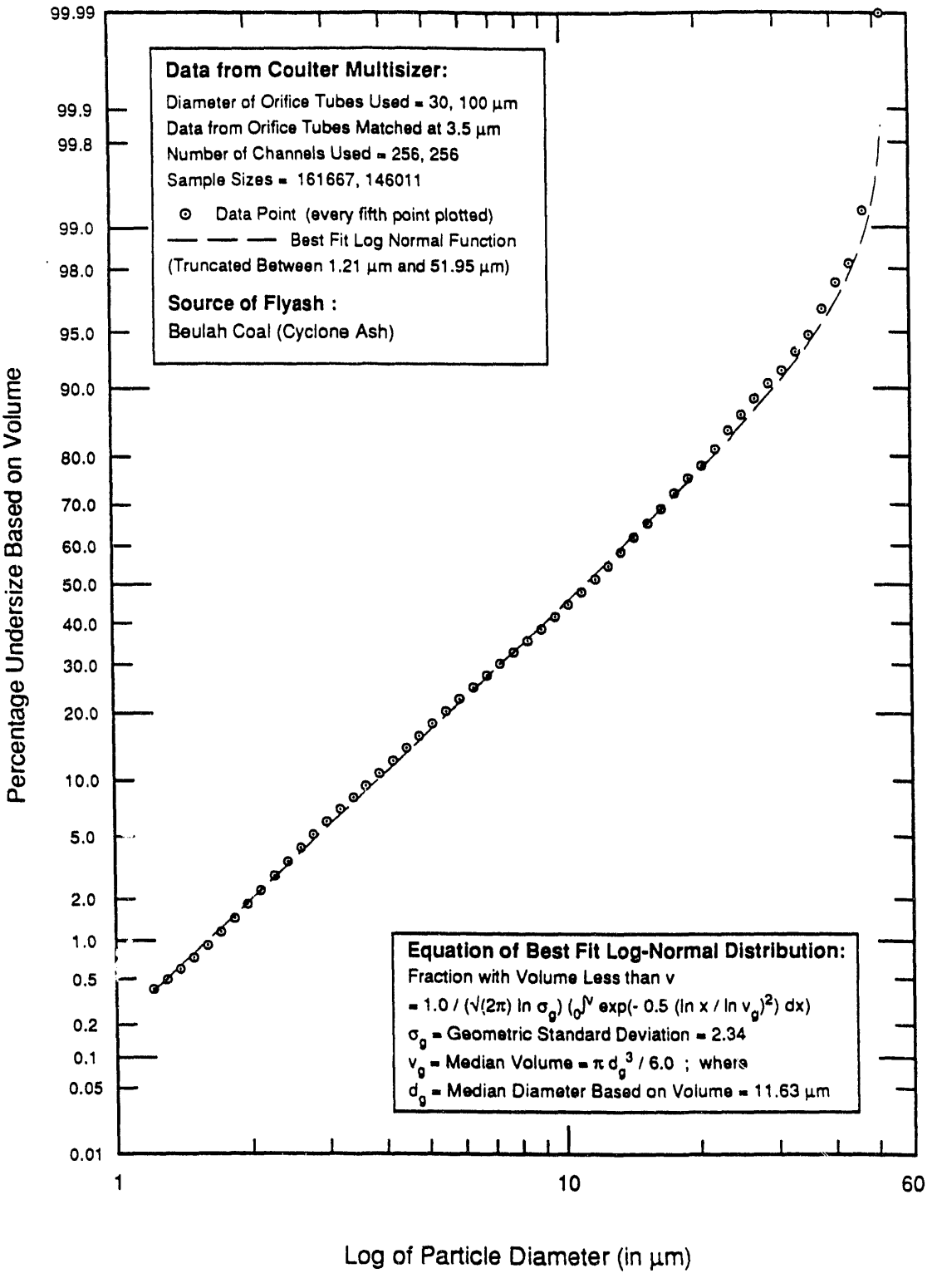

07-27-89

Figure 11

ashes from the baghouse and the upstream cyclone on the same plot. Evidently, the cyclone does not have a sharp cut-off point since it collects significant numbers of small particles. However, there are more large particles compared to the baghouse ash. The cyclone ash, therefore, has a larger median diameter. The baghouse ash contains particles with a wider range of sizes and, hence, has a larger geometric standard deviation. Both the Kentucky # 9 and the Illinois # 6 show these trends that d_V is larger and σ_g is smaller for cyclone ash, as expected. In contrast, d_V of the Beulah ash is slightly smaller for the cyclone ash.

Tabulated below are the size parameters (d_V and σ_g) for the four ashes for which sizing has been completed (Figures 5-11).

Flyash	Median Diameter Based on Volume, d_V, in μm	Geometric Standard Deviation, σ_g
Kentucky # 9 Baghouse	10.64	2.26
Kentucky # 9 Cyclone	15.67	2.02
Upper Freeport Baghouse	9.25	2.80
Illinois # 6 Baghouse	9.70	3.02
Illinois # 6 Cyclone	14.72	2.14
Beulah Baghouse	12.80	2.95
Beulah Cyclone	11.63	2.34

Density Classification:

During the past quarter, we tested various modifications to the standard centrifugal separation process [Reference 2] on controlled mixtures. The aim was to reduce the carryover of the denser fraction into the lighter fraction. This occurs because of the fluid-mechanical entrapment of heavier particles among the lighter ones as described in the last QPR. It has been found that the accuracy of the separation process, as characterized by the carryover percentage, is sensitive to the sample loading. Smaller sample masses (i.e., more dilute suspensions) produce more accurate separation. The results of a study of the effect of sample mass is tabulated below. The mixture was prepared by combining equal amounts of powdered copper sulfate crystals (density = 2.28 g/cc, color: bluish-white) and magnesium powder (density = 1.74 g/cc, color: gray). The mass median diameter of the mixture was approximately 50 μm. The liquid used in the separation was a mixture of carbon tetrachloride and dibromomethane, of density 2.0 g/cc.

Copper Sulfate (mass in g)	Magnesium (mass in g)	Total Mass (mass in g)	Percentage Carried Over
0.4827	0.5228	1.0055	34.99
0.3790	0.3740	0.7530	11.30
0.2616	0.2553	0.5169	4.89

The table shows that the carryover decreases rapidly with decreasing sample mass. However, very small samples result in proportionately greater losses in striking a mass balance. This loss was found to be less than 7% for sample masses of 0.5 g or more. Balancing these contrary factors, it has been decided to use ash sample sizes of around 0.5 g divided equally between the two centrifuge tubes. Use of different substances to prepare the test sample showed that the carryover for a fixed total sample mass varies somewhat for different sample constituents. The median particle size probably has an influence, also. For a given sample mass, smaller particles (as in the case flyash) should entrap each other to a lesser degree. However, it appears that the sample mass is the single most important factor in obtaining reasonably accurate density classification by centrifugal separation.

A typical centrifugal separation process consists of the following steps :

(a) Ultrasonically disperse 0.5 g of ash in 80 ml of the separating liquid, with a small amount of surfactant to aid deagglomeration. Divide it equally between the two 50 ml centrifuge tubes.

(b) Place the tubes in the shields and insert the latter in the trunnion rings attached to the arms of the centrifuge. Gently stir the dispersion with a thin spatula and allow for ten minutes of gravitational settling.

(c) Turn on the centrifuge and gradually increase the speed of rotation to the maximum (around 2000 rpm, corresponding to an acceleration of 1000 g) over a period of one minute. Stop after five minutes.

(d) Gently stir the float material to free any denser particles that may have got trapped. Repeat (c) for four minutes.

(e) Decant the top two-thirds of the liquid into a previously dried and weighed filter cone.

(f) Add more separation liquid to the tubes to the initial level and repeat (c) for three minutes. Now decant all the liquid into the filter paper used in (e).

(g) Extract the sink material, now embedded at the bottom of the tubes using a jet of appropriate cleaning fluid (e.g., CCl_4) from a squirt bottle and pour it into another (previously dried and weighed) filter paper.

(h) Dry, weigh and calculate the separated ash masses.

The entire operation takes about 30 minutes. It can speeded up by using more centrifuge tubes and the use of a vacuum pump when filtering.

Results of density classification of the selected ashes will be available in the next QPR.

2.1.3 Wet Magnetic Separation of Flyash:

It has been observed that there are magnetic Fe_3O_4 (magnetite) particles present in most flyashes. Since the iron in the ash plays an important role in its optical properties, it is necessary to establish the proportion of the iron present as pure magnetite particles relative to that incorporated in the glassy ash particles. This can be determined by magnetic separation of the ash samples. For this purpose we have purchased an inexpensive, manually operated separator (trade name: Automagnet) supplied by Gilson Company, Inc. It is simply a spring-loaded permanent magnet (see Figure 12). When the plunger is pressed, the magnet comes close to the separator surface, and the magnetic particles, attracted by the magnetic field at the surface, stick to the separator. It is then transferred to wherever the magnetic particles are to be deposited. When the grip on the plunger is eased, the magnet moves, and most of the particles fall off the separator. The remaining ones are washed off with distilled water from a squirt bottle.

The magnetic separation can be performed by following the steps outlined below:

(a) Ultrasonically disperse 1 to 2 gm of ash in 40 ml of distilled water with a few drops of surfactant in a beaker (beaker # 1).

(b) Move the magnetic separator, with the plunger pressed, in this dispersion (with the beaker remaining in the ultrasonic bath) for a minute.

(c) Over a larger beaker (# 2), gently wash the particles sticking to the separator surface with distilled water from a squirt bottle, while keeping the plunger pressed. The water removes the non-magnetic particles which get trapped among the magnetic ones and are picked up by the separator. A small fraction of the magnetic particles, however, is washed into beaker 2.

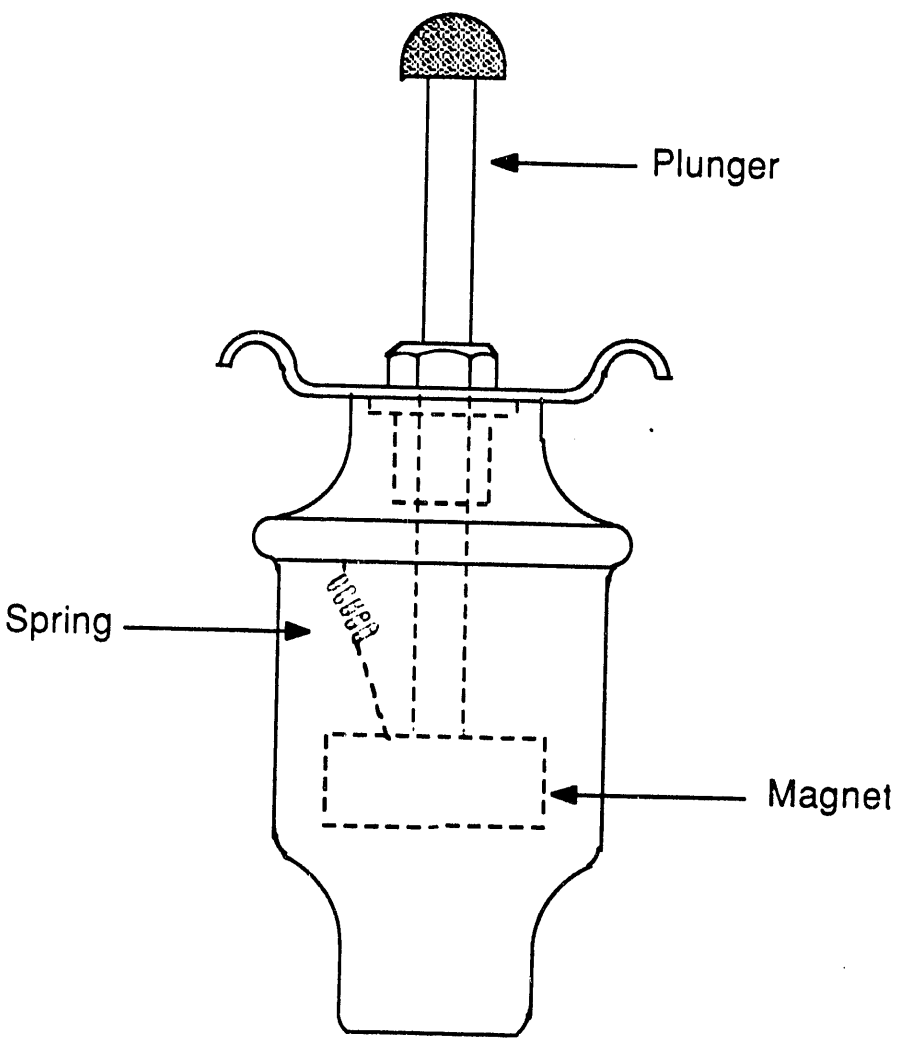

Figure 12: Magnetic Separator

(d) The separator is placed in a small amount of distilled water in another beaker (# 3) and the plunger is allowed to return to its original position. The magnetic particles, which are much heavier than water, sink to the bottom of the beaker.

(e) Repeat steps (b) and (d) for the contents of beaker 2 (wash over this beaker itself) until no more magnetic particles are being picked up in part (b).

(f) Now transfer the contents of beaker 3 to a new beaker (# 4). Beaker 4 contains all the non-magnetic flyash.

(g) Repeat Steps (b) to (f) till all the particles have been removed from the original ash dispersion.

(h) In spite of the washing in part (c), a small amount of non-magnetic particles is transferred to beaker 3 in part (d) each time. At the end, repeat steps (b) and (c) to the contents of this beaker. However, the washing is done over the same beaker. Transfer the magnetic particles to yet another beaker (# 5).

(i) Dry and weigh two quantitative filter papers. Use them to filter out the water from the two beakers (# 4 & 5). Dry the filter papers and weigh them. Now calculate the fraction of the ash that is magnetic. The non-magnetic ash mass is measured to check for mass balance.

The process is evidently iterative in nature and takes about four hours for each sample. Its precision is currently being tested. Other tests will be performed to find out the proportion of the magnetic particles that are pure magnetite particles. For a rough estimate, an EDS analysis will be performed on 30 to 40 particles picked at random from the SEM stub. If necessary, samples of magnetic particles will be sent to UNDERC for computer controlled scanning electron microanalysis (CCSEM).

2.1.4 Microanalysis by SEM/EDX:

As reported in the last QPR, samples of three ashes (Kentucky # 9, Illinois # 6, Beulah) were sent to University of North Dakota Energy Research Center (UNDERC) for CCSEM examination on a particle-by-particle basis. As requested, we received micrographs of the SEM stub along with the data. On examination of the micrographs, it was noted that most of the ash was present as large agglomerates (Figure 13a). This occurred because the 'electrostatic dispersion' method adopted by the staff at UNDERC was not suitable for the dispersion of electrically insulating flyash particles. The presence of many such agglomerates explains the large numbers of highly non-spherical 'particles' found in the CCSEM analysis. Several previous SEM studies at Stanford, reported in earlier QPRs, have established that the great majority of the ash particles are remarkably spherical. In Figures 14 and 15, are plotted the size distributions of the ash particles by number and volume

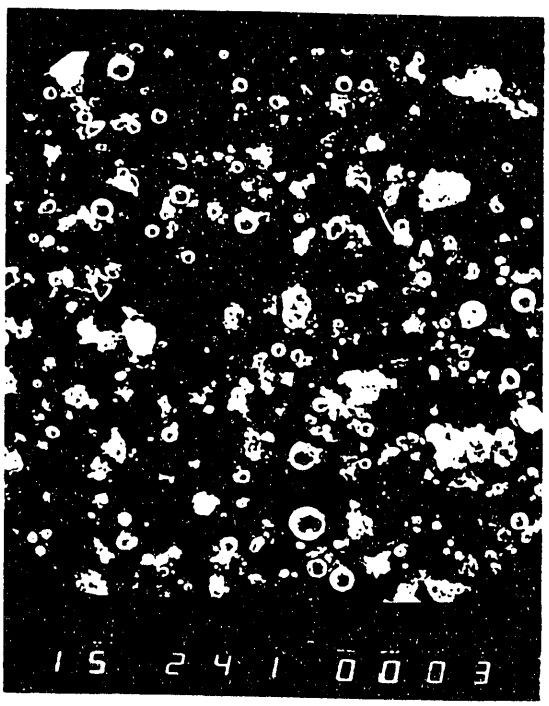

Figure 13a

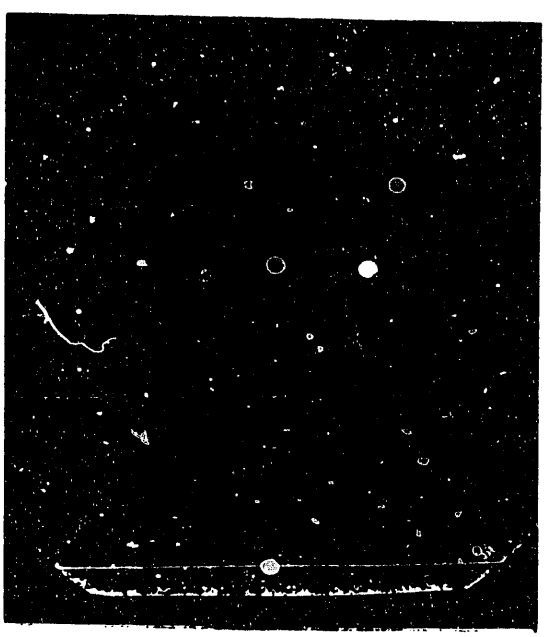

Figure 13b

Size Distribution of Flyash Plotted on Log-Probability Axes

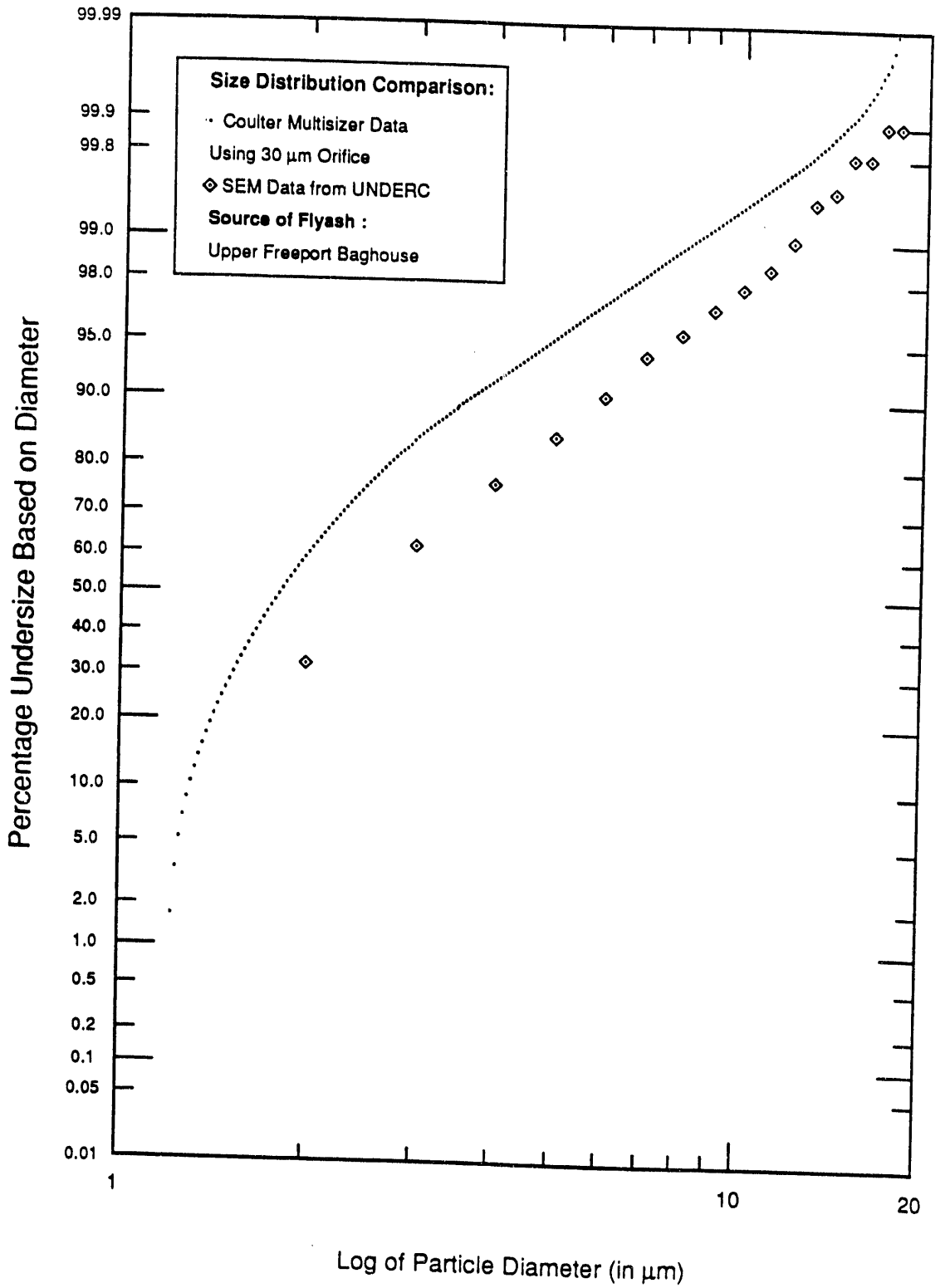

07-31-89

Figure 14

Size Distribution of Flyash Plotted on Log-Probability Axes

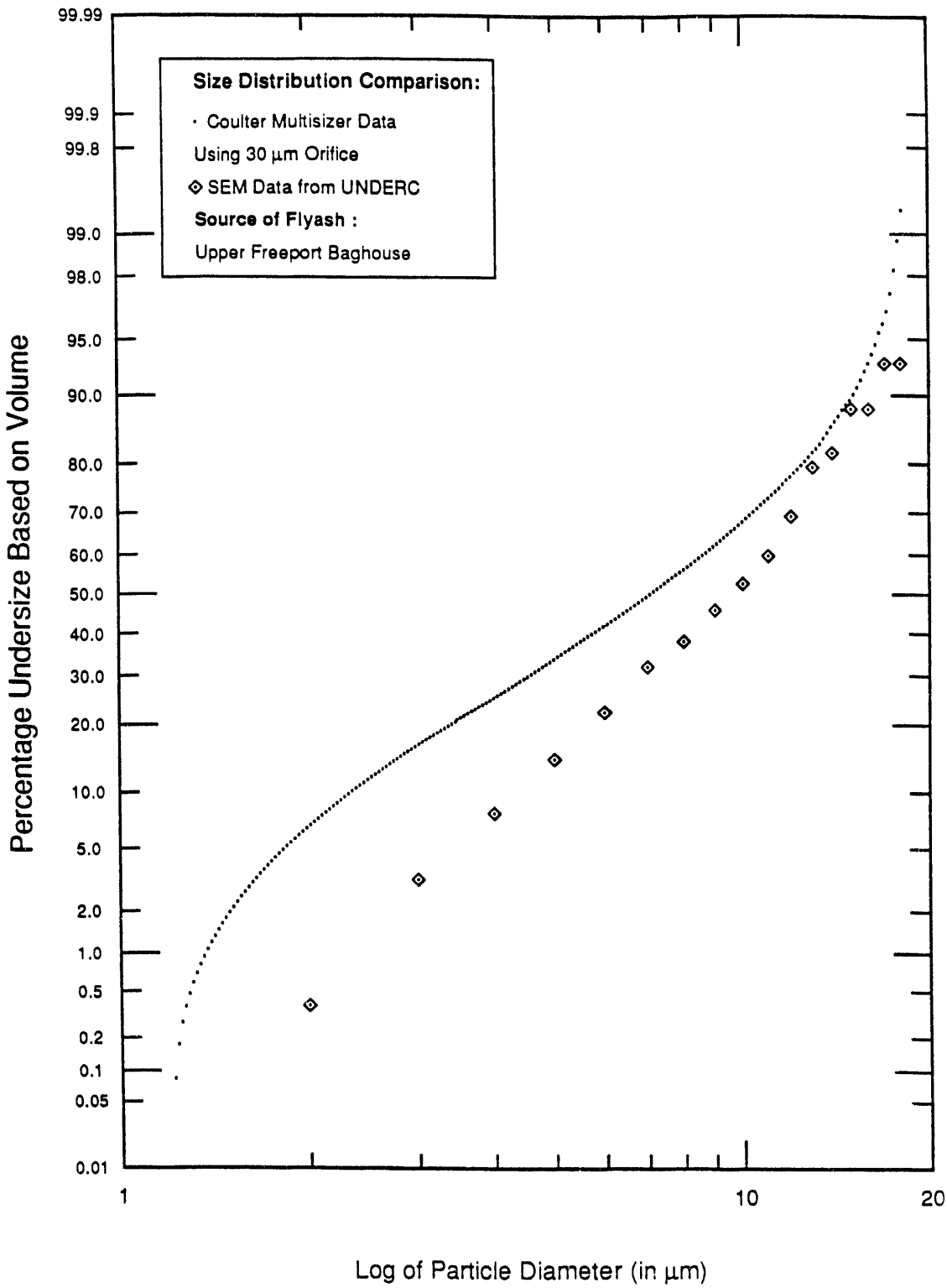

Figure 15

respectively, to compare the Coulter Multisizer data with that from the CCSEM analysis. The Multisizer size distribution takes into account all ash particles in the size range of 1.2 μm to 18.1 μm; with combined data from orifice tubes of sizes 30 μm and 100 μm. From the plots it is clear that there are far fewer small particles in the data from UNDERC. While a small statistical discrepancy arises from the fact that only 1000 particles were examined at UNDERC compared to over 100,000 particles sized by the Multisizer, most of the difference in the two size distributions can be attributed to the presence of large agglomerates in the CCSEM sample. This has rendered the CCSEM data on the four ashes (Upper Freeport ash and the three mentioned above) analyzed so far to be of questionable value. In the past quarter, we have developed a technique for dispersing ash on a SEM stub to an adequate degree, as described below in detail. It has been decided that we will prepare the ash samples on carbon stubs using this technique and mail them to UNDERC for analysis. Currently, we are awaiting the results of the repeat analyses of the last three ashes, using well deagglomerated samples prepared at Stanford.

Preparation of Ash Sample for SEM Analysis :

It is impossible to prepare adequately deagglomerated ash samples in a dry state by any known method. We have developed a method of sample preparation by freeze-drying a liquid suspension of ultrasonically dispersed ash. A brief reference to the freeze-drying technique for SEM sample preparation, without any description or further reference to the procedure can be found in Reference 3.

Ash Dispersion: The criteria for choosing a liquid for dispersing the ash are (a) a high freezing point; (b) low surface tension to allow the liquid drops to spread evenly over the stub surface; (c) fairly high vapor pressure (solid in contact with its own vapor) so that the dispersant sublimes in a reasonable time (d) miscibility in water (d) low viscosity so that particles move around more easily when agitated ultrasonically and disperse better and, finally, (f) easy availability. Two liquids found suitable for our purpose are acetone (C_3H_6O) and carbon tetrachoride (CCl_4) whose properties [Reference 4] are tabulated below:

Property	Acetone	CCl_4
Freezing Point (in °C)	−94.0	−22.6
Surface Tension (dynes/cm) at vapor-liquid interface	23.7 @ 20°C	26.95 @ 20°C
Vapor Pressure (mm of Hg)	400 @ 39.5°C	100 @ 20°C
Viscosity (centipoise)	0.316 @ 25°C	0.969 @ 20°C
Miscible in water ?	Yes	Yes

Initially, about 0.6 g of the ash is dispersed in approximately 10 ml of distilled water in a small beaker with 10 to 12 drops of surfactant (all 'drops' in the report refer to drops from a standard eye-dropper) and placed in an ultrasonic bath (nominal output frequency: 50 kHz) for five minutes. Next, about a dozen drops of the suspension is transferred, using the eye-dropper, to another small beaker containing 10 ml of acetone or carbon-tetrachloride and again ultrasonically agitated. The ash particles are now well dispersed and ready for freeze drying.

A sketch of the of the freeze drying apparatus is shown in Figure 16. Before the liquid nitrogen is poured into the styrofoam bath, the chamber is pumped down to prevent moisture from the air condensing on the stub. The liquid nitrogen cools the aluminum block and the stub to a temperature below the freezing point of the dispersing liquid in five to ten minutes depending on the size of the block and the quality of the thermal contact between the stub surface and the block. More liquid nitrogen is added, as needed, since the initial charge boils off rather quickly. Once the stub surface is sufficiently cooled, the glass cylinder is gently prised loose at the O-ring-aluminum block contact point. Two to three drops of the suspension is placed on the stub surface and the cylinder is replaced on the block. The vacuum pump is operated continuously. The exposure of the stub surface to the atmosphere should be kept short to minimize condensation of atmospheric moisture. Additionally, some gaseous nitrogen may be directed towards the stub during the exposure. The liquid should freeze within three to four seconds; if it takes longer, it indicates that the stub had not cooled sufficiently. The set-up is now left for an hour or so, during which time the solidified dispersant (mainly acetone or carbon tetrachloride with a small amount of water and surfactant) sublimes. The transparent cylinder allows one to see that all the solid has sublimed. The stub and the block are now warmed to room temperature (e.g., with a heat gun) before the pressure is raised to atmospheric to prevent condensation of water vapor from the air on the stub. The stub is now ready to be coated and examined under the SEM. Figure 13b shows a typical sample prepared in this manner.

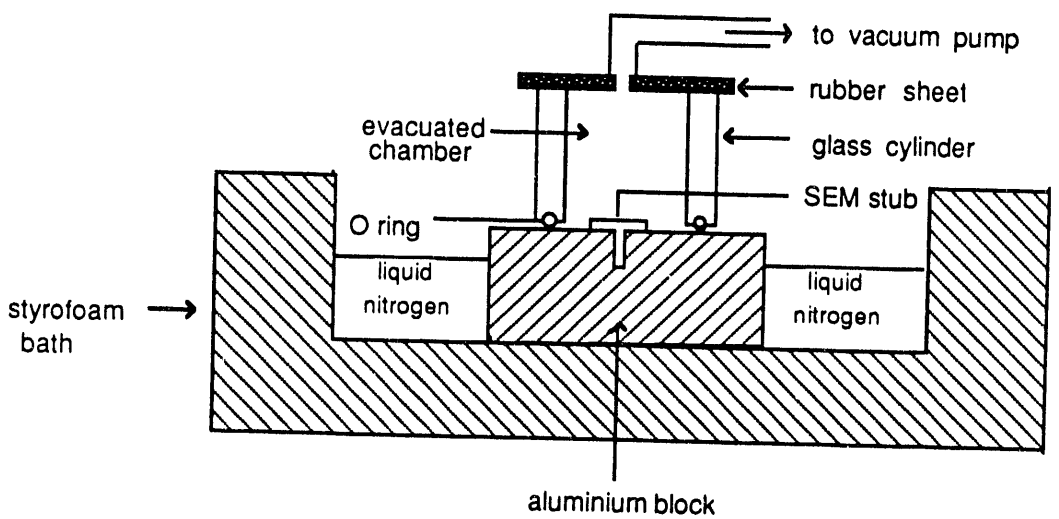

Figure 16: Section of Set-up for Preparing Sample for SEM Analysis

2.2 Task 2: Optical Properties of High Temperature Slag

The immediate goal of this task is to measure the high temperature optical properties of coal slag. The complex refractive index, $m = n - ik$, will be measured for synthetic slags at temperatures near 1900 K. The effect of composition on the optical properties will be investigated.

As established in the earlier work of Goodwin [5] on solid slag samples, two separate techniques are required to determine n and k over the whole wavelength range from the visible to $\lambda \sim 12\ \mu m$. For $\lambda \leq 5\ \mu m$, where k is small enough ($< 10^{-2}$) that the transmission T of a thin, optically polished wafer (thickness h) is not too small to allow accurate measurement, the absorption index, k, can be found from the formula

$$T = exp(-4\pi kh/\lambda) \tag{1}$$

When k is known, the real index, n, can be found from measurement of the near normal reflectance, R_n, using the Fresnel formula

$$R_n = \frac{(n-1)^2 + k^2}{(n+1)^2 + k^2} \tag{2}$$

For $\lambda < 5\mu m$, n can be found from the measured values of R_n using Eq(2) with the values of k determined from the measured values of T using Eq(1).

For $\lambda \geq 5\mu m$, where k is too large to allow transmittance measurements, values of n and k may both be inferred solely from reflectance measurements (provided they are made over a large enough wavelength range) by use of the Kramers–Kronig relations which are analytic formulas relating n and k in integral forms. The Kramers–Kronig relations are

$$n(\omega) - 1 = \frac{2}{\pi} P \int_0^\infty \frac{\omega' k(\omega')}{\omega'^2 - \omega^2} d\omega' \tag{3}$$

and

$$k(\omega) = -\frac{2}{\pi} P \int_0^\infty \frac{n(\omega')}{\omega'^2 - \omega^2} d\omega' \tag{4}$$

where ω is frequency and P denotes the Cauchy principal values of the integrals.

For high temperatures, when the slag is molten, the same two basic methods may be used, but the experimental techniques must be modified. Also, since the measurements must be made with the sample inside a high temperature furnace, considerable technical difficulties must be overcome.

To measure the absorption index, we are using a "submerged reflector" technique whereby a platinum mirror is suspended just below the liquid surface and the absorption index is measured by a double pass through the thin, overlying slag layer. By measuring the change in absorption when the mirror is displaced by a small increment Δh, the absorption index can be found from the change in transmission from the formula

$$\frac{T_{h+\Delta h}}{T_h} = exp\left(-\frac{4\pi k(2\Delta h)}{\lambda}\right) \tag{5}$$

without having to know the reflectivity of the platinum mirror.

As reported in a previous QPR, we have successfully implemented this technique and made measurements of k on a synthetic slag containing 5% Fe_2O_3 (SA05) at 1600°C over the range $1 \leq \lambda \leq 5\mu m$. The measurements are in accord with those of Goodwin on slag of the same composition at lower temperatures.

In the last QPR we reported progress on the near normal reflectance measurements. Figure 17 illustrates the optical system for measuring near normal reflectance. The broadband source (Nernst Glower) is first imaged onto the aperture to reduce the size of the image inside the furnace and reduce unwanted spurious light. The aperture is larger than the 1 mm square detector area, the field stop for the optical system. After the aperture, the chopper modulates the beam at 670 Hz to allow synchronous detection of the signal from the HgCdTe infrared detector with a Stanford Research Systems SR530 lock–in amplifier. The gold mirror M4 is movable to allow the spherical concave mirror M3 to image the source onto either the sample (inside the furnace) or onto the gold reference mirror. Concave mirror M5 collects the reflected beam and focuses it onto the entrance slit of the monochromator. Low pass filters in front of the entrance slit prevent higher order wavelengths from being detected. Four different gratings are used to span the entire wavelength range $1 \leq \lambda \leq 14\mu m$.

Measurements of the near normal reflectance of a slag wafer placed inside the cold furnace agreed very closely with Goodwin's results. To check the technique at high temperature,

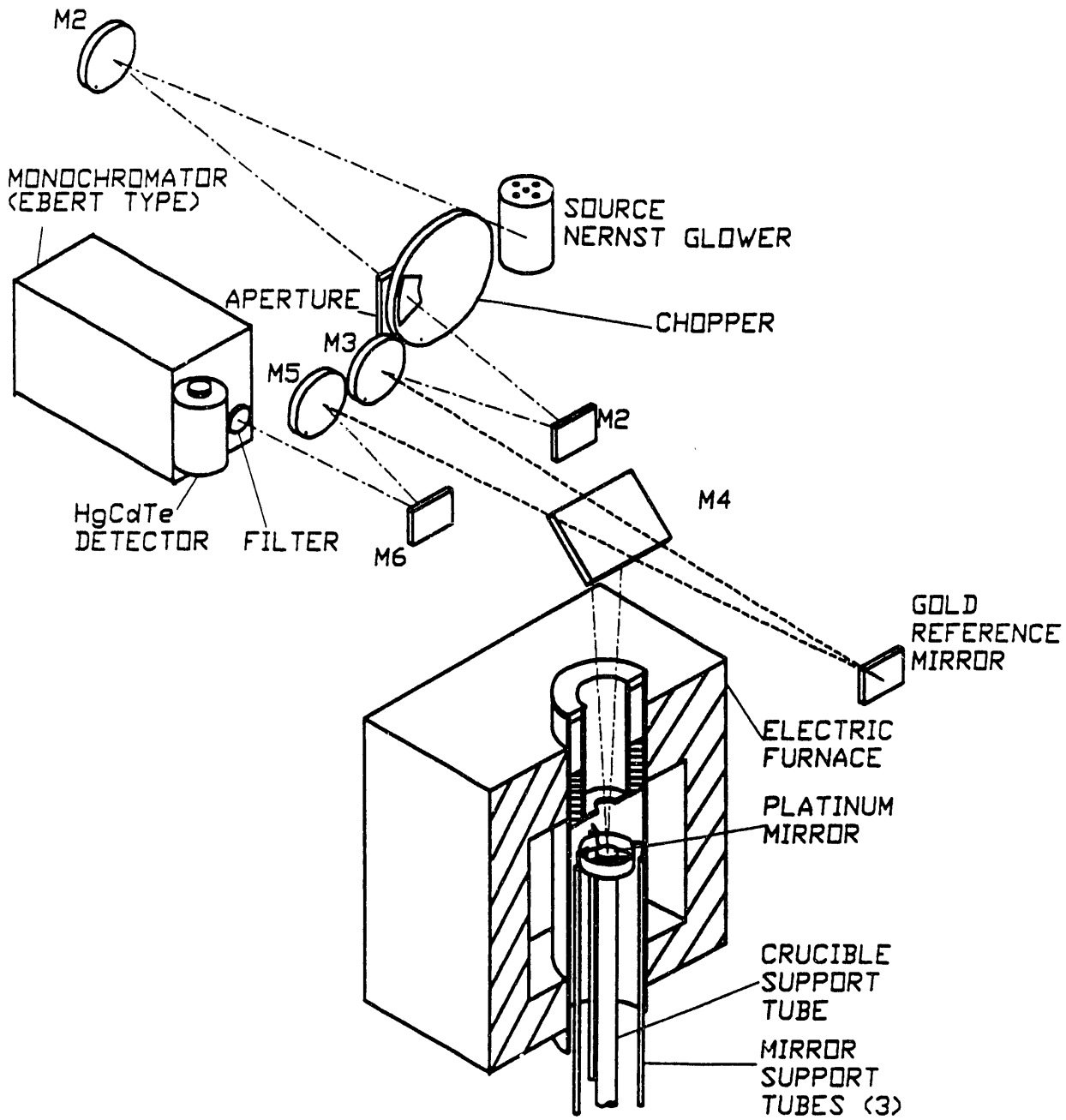

Figure 17. Schematic of the optical system for high temperature reflectance measurements.

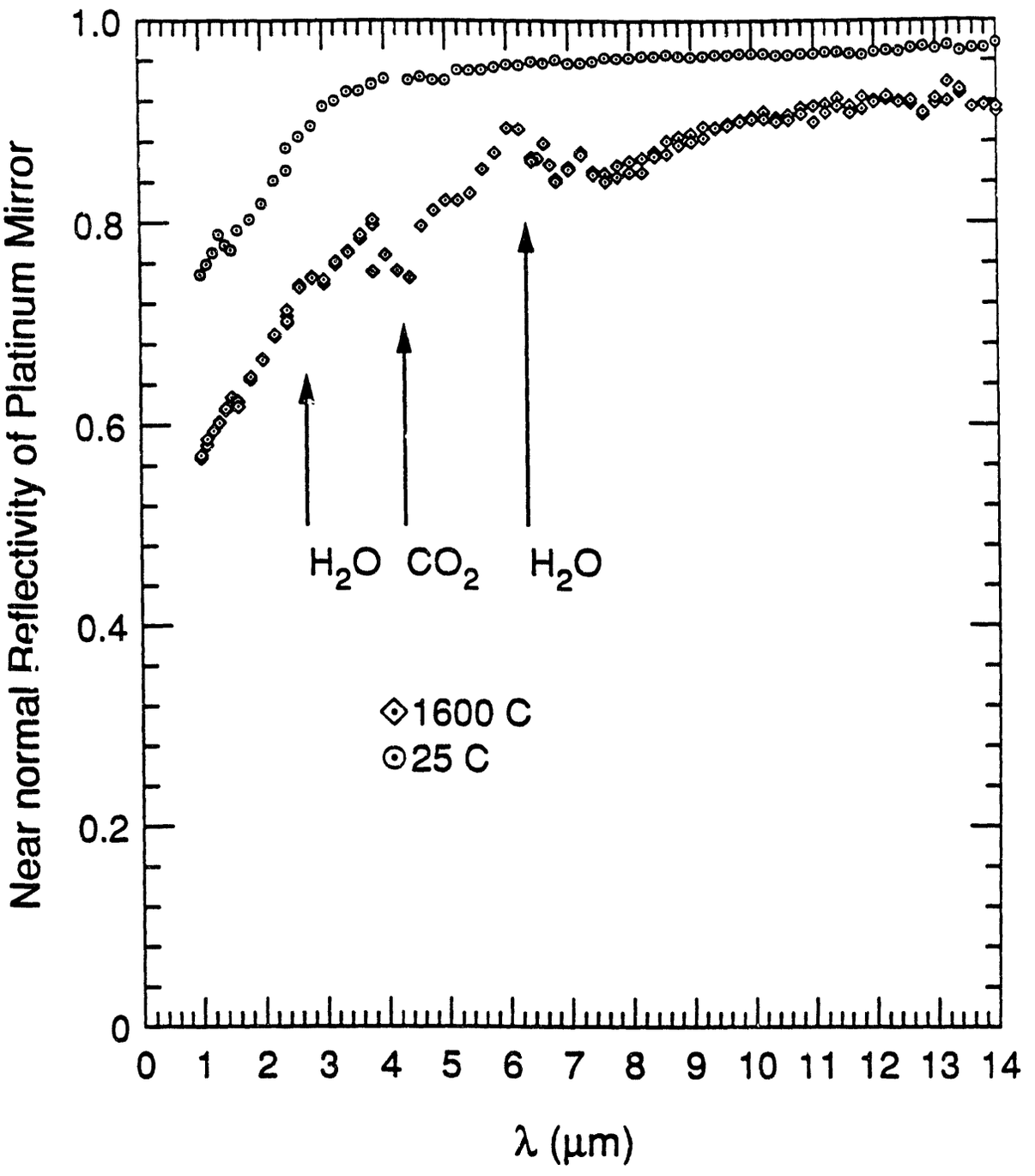

Figure 18. Reflectance of a platinum mirror showing the effect of atmospheric absorption bands on the high temperature measurements.

reflectance measurements of platinum were made. An experiment was reported in which near normal reflectance measurements were made of the platinum mirror supported inside the furnace. The reflectance measurements for room temperature platinum agreed very well with published data for platinum. Following the cold test; the measurements were repeated with the furnace at $1600°C$. However, the strong CO_2 and H_2O absorption bands in the room air were found to significantly affect the measured reflectance — the difference in the transmittance of the cold air in the reference path and the hot air in the sample path was being convolved with the sample reflectance. Figure 18 shows the results of these measurements with the positions of the strongest absorption bands identified.

Two methods for removing the unwanted interference due to differential gas band absorption on the slag reflectivity measurements were apparent. The first involved computing the differential gas band absorption in the cold and hot paths and using this to correct the measured data. This was rejected in view of the difficulty of calculating the gas band absorption with sufficient accuracy. The second, more direct method was to eliminate the CO_2 and H_2O absorption by purging the optical paths with dry nitrogen.

During the past quarter we have concentrated our efforts on removing the CO_2 and H_2O bands from the optical system. A hood has been constructed to fit over the entire optical system so that nitrogen can be used to purge the infrared active gases. This considerable reconstruction of the optical system is now complete and several measurements have been made.

When the hood is sealed, liquid nitrogen is boiled and heated to about 30°C through copper tubing in a heated water bath. A rotameter allows control of the flow rate to a maximum near 200 $ft^3/hour$. The volume of the hood is approximately 40 ft^3 and can be adequately purged in about 3 hours, after which the nitrogen flow rate is decreased to approximately 40 $ft^3/hour$ to decrease the flow rate through the furnace. A small fan under the hood is used to circulate the nitrogen, and an air cleaner (Norelco Clean Air Machine) is used to remove dust from the gas. The nitrogen flows from the hood into the furnace tube and exits the bottom of the furnace; therefore, the air cleaner is necessary to prevent dust particles from impacting and sticking to the hot sample.

By monitoring the detector signal at the wavelength of 4.24 μm, we are able to determine when the purging is complete. Figure 19 shows that it takes approximately 3 hours to reduce the CO_2 absorption to insignificant levels. Figure 20 shows the signal over the 4.3 μm CO_2 band and the 2.7 $\mu m H_2O$ band at several times during the purge. It is seen that while most of the CO_2

is removed, some water vapor remains in the system even after 8 hours of purging. However, the water vapor concentration is low enough to allow accurate high temperature reflectance measurements of molten slag.

During the past quarter the reflectivity of a platinum mirror was measured again but with the system purged with nitrogen. Figure 21 shows the measured reflectivity for the platinum mirror at 1550° C and, as expected, the effects of the atmospheric absorption bands are removed.

The high temperature measurements show considerably more noise than do the room temperature measurements. There are several possible explanations for this, but the most likely explanation is that the strong thermal gradients in the column above the furnace cause density gradients which steer the beam across the monochromator entrance slit. This causes low frequency changes in the detected signal which cannot be removed by the lock-in amplifier.

The reduction in the reflectivity is somewhat greater than we should expect based on a temperature difference only. For metals we expect the reflectivity to vary roughly as described by the Hagen–Rubens relation

$$R \simeq 1 - 2(0.003\lambda/r_e)^{-1/2} \tag{6}$$

where r_e is the electrical resistivity of the metal in $\Omega \cdot cm$ and λ is the wavelength in μm . The electrical resistivity can be approximated by $r_e \sim r_{e,293}T/293$ ($r_{e,293} \sim 10 \times 10^{-6}\Omega \cdot cm$ for Pt) to give the approximate relation

$$R \simeq 1 - \frac{2(r_{e293}\frac{T}{293})^{1/2}}{(0.003\lambda)^{1/2}} \tag{7}$$

where T is temperature in Kelvins. Figure 21 shows this approximation for $T = 1550°$ C (1823 K). Since the Hagen–Rubens relation is only valid for long wavelengths, it is not surprising that it does not match the data very well for $\lambda \leq 5\mu m$. For longer wavelengths it does accurately predict the shape ($1 - R \propto \lambda^{-1/2}$) but the measured reflectivity is about 10% lower than the predicted value. This difference may be explained by surface roughness of the platinum mirror. When the platinum mirror is heated to 1550° C there is considerable grain growth which causes the polished mirror to become rough. The grains are irregularly shaped regions outlined by grain boundaries in the form of grooves. The grains range in size from 20 μm to 500 μm or so. Within each grain there are small hemispherical pits in the surface with sizes on the order of

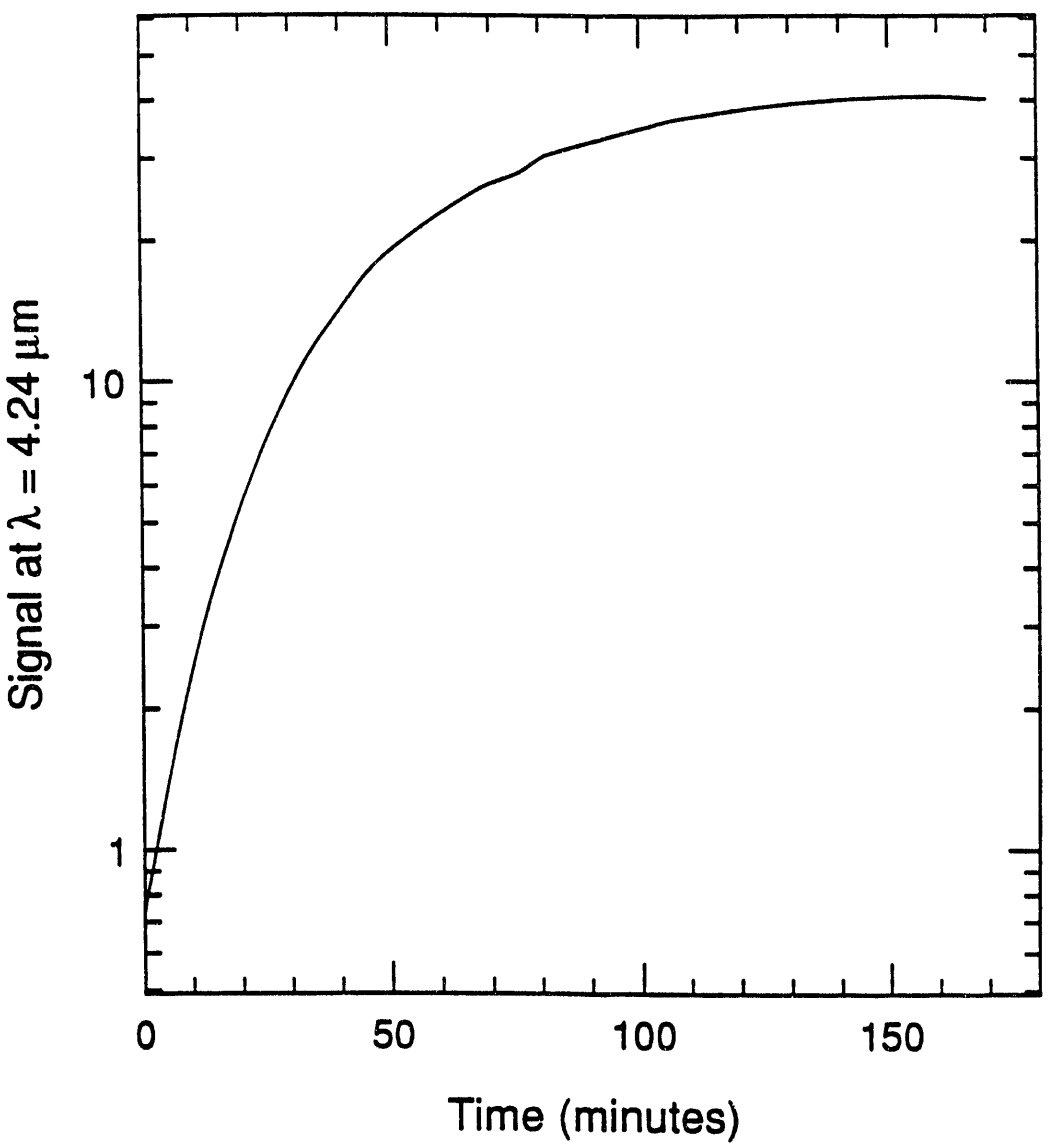

Figure 19. Detector signal at 4.24μm during a nitrogen purge of the optical system.

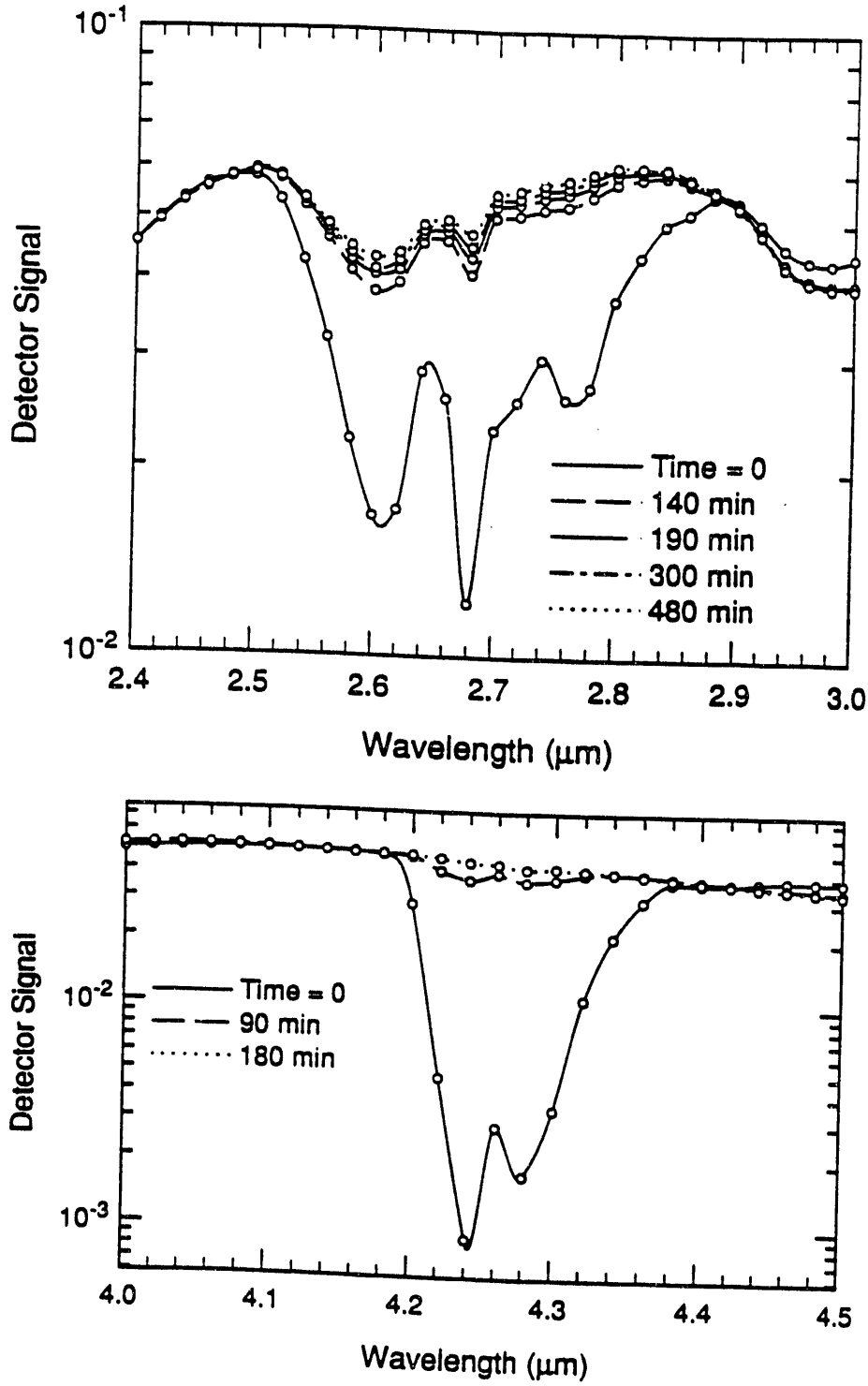

Figure 20. Detector signal across the $4.3\mu m$ CO_2 band and the $2.7\mu m$ H_2O band at various times during a nitrogen purge of the optical system.

a few microns. The effect of this increased roughness is to produce scattering and reduce the specular reflectivity of the mirror. Since the detector area is a 1 mm square, several grains are imaged simultaneously, giving an averaged reflectivity.

Next the furnace was cooled and the platinum mirror was replaced by a 50 ml alumina crucible of slag SA05 (5% Fe_2O_3 by wt.) which was prepared earlier for use in the submerged reflector experiments. The 50 ml crucible has a $60mm$ ID which is large enough to provide a flat liquid surface despite the efforts of surface tension to curve the surface. The slag was heated to 1600°C and carefully positioned inside the furnace. The molten slag was approximately 1 cm thick, thus absorbing any light that entered the slag. Only the portion of the beam which was reflected from the molten surface was collected. The system had been purged with nitrogen continuously for approximately 20 hours when the slag reflectance measurements began and the measurements took approximately 4 more hours to complete. However, there was still a small but measurable absorption by the 2.7 μm H_2O band after purging for nearly 24 hours.

The reflectance of the synthetic slag SA05 is shown in Figure 22. The noise which was evident in the platinum reflectance is significantly reduced in this data. This seems to give credence to the idea that the combination of surface roughness and beam steering is responsible for much of the noise in the platinum reflectance measurement. Also shown in Figure 22 is the room temperature reflectance of a similar slag calculated using Goodwin's [5] data for n and k. The agreement in the region $\lambda < 8\mu m$ is quite good, as expected. In this region k is small, and the reflectance (see Eq(2)) is almost entirely due to n, and n is expected to decrease only slightly with increasing temperature due to the density decrease.

The Kramers–Kronig relations were used to reduce the near normal reflectance data to yield n and k. The expressions in equations (3-4) are not directly useful here but alternate forms can be derived in terms of a reflection coefficient r and a phase shift on reflection θ_R. The reflection coefficient r is related to the reflectance by $R = |r|^2$ and the phase shift is defined as $r = |r|exp(i\theta_R)$. In this form we have

$$\theta_R(\omega) - \pi = -\frac{\omega}{\pi} P \int_0^\infty \frac{ln\, R(\omega')}{\omega'^2 - \omega^2} d\omega' \tag{8}$$

Once $\theta_R(\omega)$ is computed using a sufficiently wide wavelength range of reflectance R data, n and k are computed using the relations

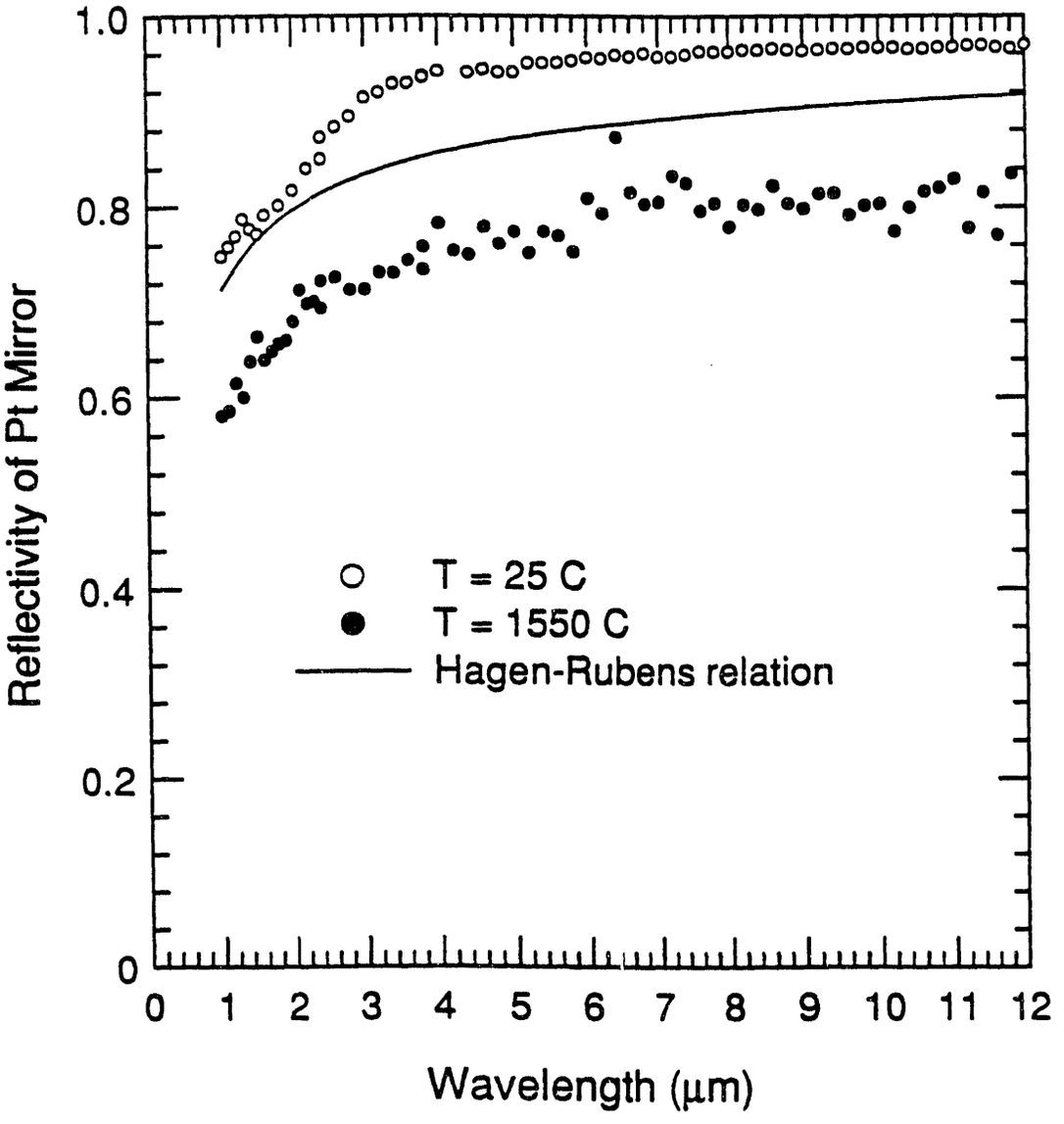

Figure 21. Reflectivity of platinum mirror measured in the nitrogen environment.

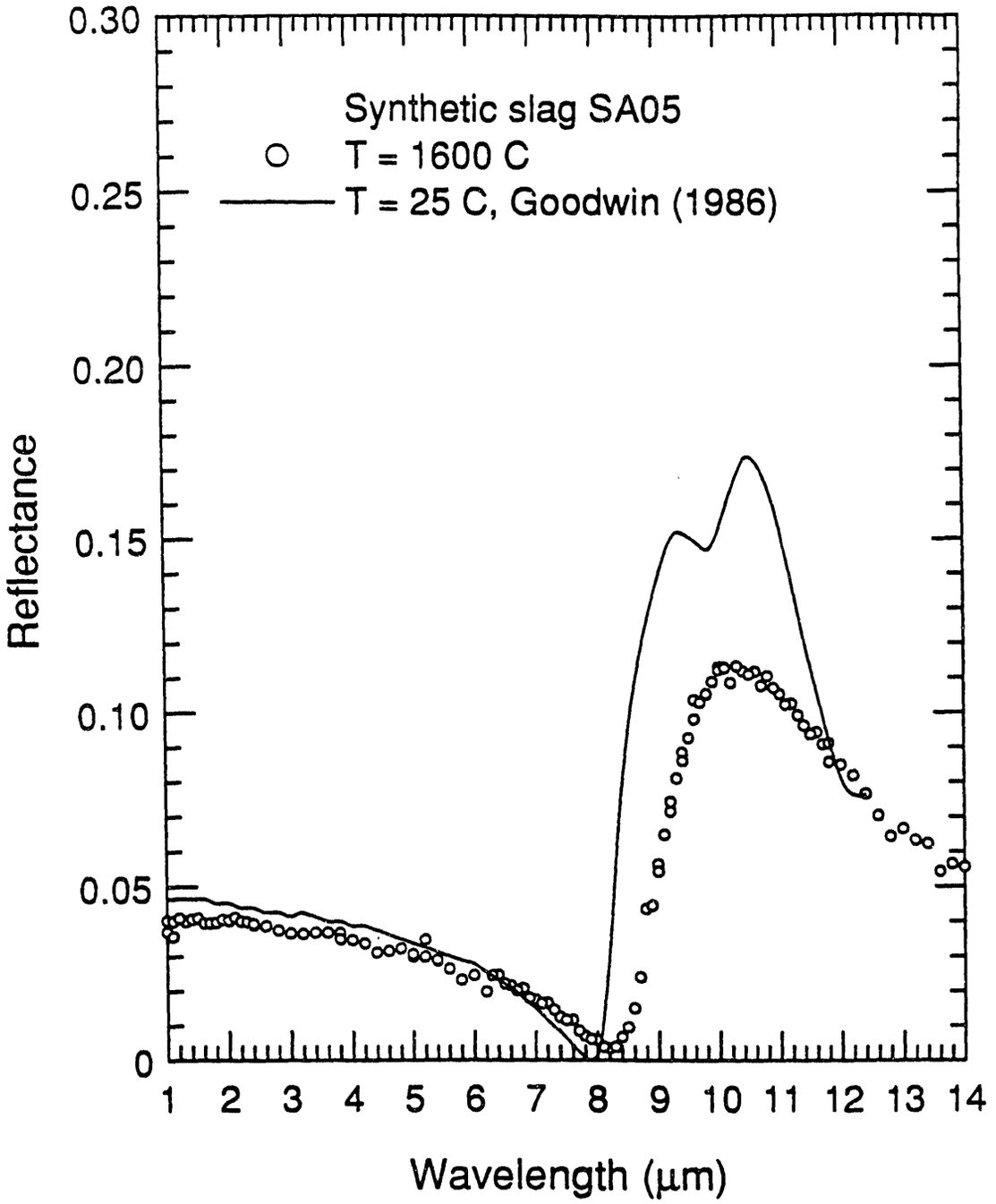

Figure 22. Reflectance of slag SA05 (5% Fe_2O_3) at 1600°C compared to room temperature measurements of Goodwin (1986).

$$n = \frac{1 - R}{1 + R + 2\sqrt{R}\cos\theta_R} \tag{9}$$

$$k = \frac{-2\sqrt{R}\sin\theta_R}{1 + R + 2\sqrt{R}\cos\theta_R} \tag{10}$$

A computer program was written to compute n and k from this reflectance data using the Kramers–Kronig relations. The integral shown in equation (9) can be evaluated analytically outside the wavelength range for which we have data by assuming the reflectivity is constant outside the range of available data. That is, assume

$$R(\omega) = R(\omega_a), (\omega \leq \omega_a) \tag{11a}$$

$$R(\omega) = R(\omega_b), (\omega \geq \omega_b) \tag{11b}$$

where $\omega_a \leq \omega \leq \omega_b$ is the frequency range of the available reflectance data. By subtracting $ln\, R(\omega)/(\omega'^2 - \omega^2)$ from the integrand of equation(8), which is allowed since $\int_0^\infty 1/(\omega'^2 - \omega^2) = 0$, the integrand becomes finite and can be computed easily. The resulting expression for the phase shift is

$$\begin{aligned}\theta_R(\omega) - \pi = & \frac{ln(R(\omega_a)/R(\omega))}{2\pi}\, ln\left|\frac{\omega + \omega_a}{\omega - \omega_a}\right| \\ & + \frac{ln(R(\omega_b)/R(\omega_b))}{2\pi}\, ln\left|\frac{\omega_b - \omega}{\omega_b + \omega}\right| \\ & - \frac{\omega}{\pi}\int_{\omega_a}^{\omega_b} \frac{ln\, R(\omega') - ln\, R(\omega)}{\omega'^2 - \omega^2} d\omega'\end{aligned} \tag{12}$$

Figure 23 shows the reduced results for n and k from the Kramers–Kronig analysis discussed above. In addition to the reduced results, the previously reported result for k in the $1 \leq \lambda \leq 5\mu m$ by double–pass absorption is shown. The Kramers–Kronig (KK) method cannot be used to obtain k for k less than about 0.1; therefore, there is a gap in the k data between 5 μm and

8 μm . This limitation does not affect finding n using the KK method. Since the phase shift is very near π for $k \sim 0$ Eq(9) is approximately equivalent to

$$n \simeq \frac{1-R}{1-2\sqrt{R}+R} = \frac{1-\sqrt{R}}{1+\sqrt{R}} \tag{13}$$

which is also directly derivable from the Fresnel formula, Eq(2), for $k = 0$. It is easily shown that the limitation of $k \geq 0.1$ is also a limitation in using equation(2) for determining k from n and R, since as k becomes small, the resulting expression requires computing a small difference between two large numbers.

The results in Figure 23 show a marked effect of temperature on both k and n. We see that the Christiansen wavelength (where $n = 1$) is shifted to slightly longer wavelengths at higher temperatures. Also, both n and k decrease with increased temperature in the wavelength range from 8 μm to 11 μm . The Restrahlen absorption band above 8 μm appears to be broadened at elevated temperatures.

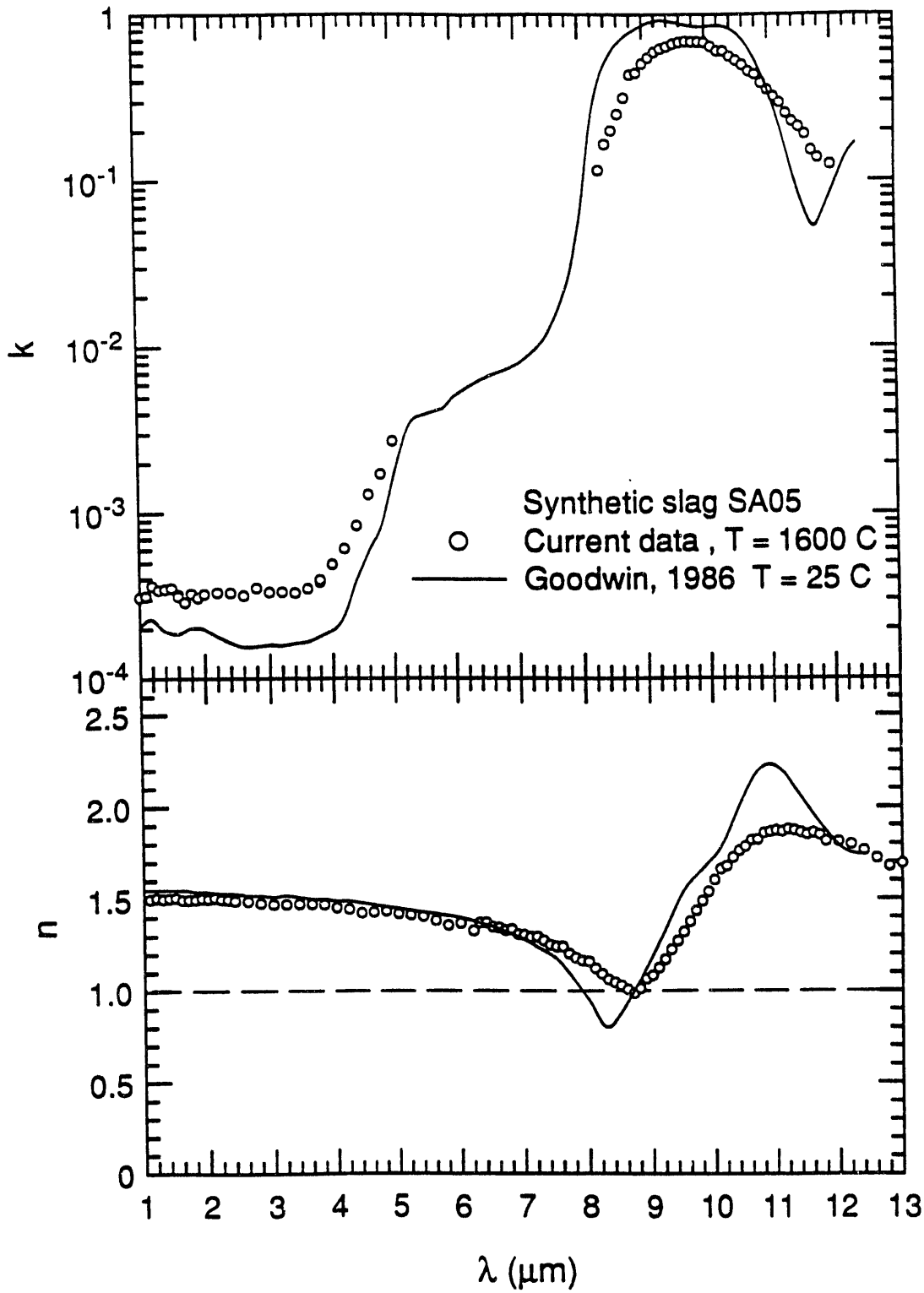

Figure 23. Complex refractive index of slag SA05 (5% Fe_2O_3) at 1600°C compared to room temperature measurements of Goodwin (1986). Data for k and $\lambda \leq 5\mu m$ was obtained by the submerged reflector technique.

2.3 Task 3: Sample Calculations of the Radiant Properties of Flyash Dispersions

During the past year, several computer codes have been developed for this task. They were used to compute the effect on radiant transfer of varying the distribution of the iron content with particle size as reported in a paper presented at the Engineering Research Foundation Conference on "Mineral Matter and Ash in Coal" at Santa Barbara. These codes are also being used to determine the design conditions for Task 4.

2.4 Task 4: Measurement of the Radiant Properties of Flyash Dispersions

As noted earlier, the purpose of this task is to validate the whole approach adopted in this program. Specifically, this bench-scale experiment is intended to compare the measured optical/radiative properties of a dispersion of well characterized ash with those calculated on the basis of the known size/composition distribution using the correlation formulae relating the composition and complex refractive index resulting from measurements on bulk samples of synthetic slag (Task 2).

During the past two quarters, considerable thought has been given to the various possible approaches to satisfying the objectives of this task. Several experiments were done during the past quarter to guide our design of an apparatus for measuring the scattering and absorption properties of dispersions of flyash.

As a result of these experiments, and from extensive prior experience in connection with research on electrostatic precipitation, it has been determined that there is no satisfactory way to satisfy the aims of this task using a gaseous dispersion of flyash because it is not possible to adequately disperse and deagglomerate flyash into a gas stream. Unless the ash is adequately dispersed, as it exists in the radiant boiler of a pulverized coal-fired combustion system, one cannot expect calculations, based on Mie calculations for a dispersion of spheres to properly agree with laboratory measurements.

For these reasons, our design efforts for Task 4 are based on making measurements on a dispersion of flyash in liquid, for which our experience shows we can obtain stable, well-deagglomerated dispersions of ash. Because there is not single liquid which is adequately transparent over the wavelength range 1–12 μm, we plan to use a combination of three liquids, $C Cl_4$, $C S_2$ and bromoform to cover the full range. Windows of BaF_2 will be used to contain the liquid suspension in an absorption/scattering cell.

A small flow loop, incorporating the measurement cell, an ultrasonic bath and a peristaltic pump is being assembled for this work which will employ the same infrared optical equipment used for measurements on slag samples under Task 2.

Calculations are being made to determine the ash loading required in the liquid suspension to yield extinction values, E, in the range 3–30%. The lower limit is set by the accuracy of measuring the transmission T = (1–E) by ratioing the transmitted infrared signals with and without particles present in the cell. The upper limit is set by the need to restrict measurements to the single-scatter regime, so as to avoid the complication of allowing for multiple scatter i.e. radiation transfer calculations. Because the extinction may be expected to vary widely over the full wavelength range, it will probably be necessary to adjust the ash loading in the liquid in different wavelength ranges.

3.0 REFERENCES

[1] W. H. Press, B. P. Flannery, S. A.Teukolsky, W. T. Vetterling, 'Numerical Recipes: The Art of Scientific Computing', Cambridge University Press, 1986.

[2] J. S. Browning, 'Heavy Liquids and Procedures for Laboratory Separation of Minerals', USBM Information Circular No.8007, 1960.

[3] P. B. DeNee, 'Collecting, Handing and Mounting Particles for SEM', Scanning Electron Microscopy, 1978, Volume 1, pp. 479-485.

[4] CRC Press, 'Handbook of Chemistry and Physics', 60^{th} Edition, 1980.

[5] Goodwin, D. G., "Infrared Optical Constants of Coal Slags," Ph.D. Thesis, Topical Report T-255, High Temperature Gasdynamics Laboratory, Mechanical Engineering, Stanford University, (1986).

END

DATE FILMED

12 / 15 / 92